Functional characterization of the 9q34.13 locus identifies *RAPGEF1* as modulating risk for melanoma and nevi via RAS activation

Rohit Thakur[1,*], Mai Xu[1,*], Alexandra M. Thornock[2,3,4,5], Joshuah Yon[1], Samuel Anyaso-Samuel[6], Martin Lauss[7,8], Thomas Rehling[1], Linh Bui-Raborn[1], Hayley Sowards[1], Gerard Duncan[9], Lea Jessop[10], Timothy Myers[10], Raj Chari[11], Erping Long[1,12], Karen Funderburk[1], Jinhu Yin[1], Rebecca Hennessey[1], Emory Hseih[1,13], Hannah Levin[1], Mitchell J. Machiela[14], Tongwu Zhang[14], Goran Jonsson[7,8], D Timothy Bishop[15], Julia Newton-Bishop[16], Jeremie Nsengimana[17], Mark M. Iles[16,18], Maria Teresa Landi[14], Matthew H. Law[19,20,21], Thorkell Andresson[9], Jiyeon Choi[1], Leonard I. Zon[2,3,4], Jianxin Shi[6], Melanoma Meta-Analysis Consortium[22], Kevin M. Brown[1,#]

[1]Laboratory of Translational Genomics, Division of Cancer Epidemiology and Genetics, National Cancer Institute, Bethesda, MD, 20892, USA
[2]Stem Cell Program and Division of Hematology/Oncology, Boston Children's Hospital and Dana Farber Cancer Institute, Howard Hughes Medical Institute, Boston, MA, USA
[3]Stem Cell and Regenerative Biology Department, Harvard University, Cambridge, MA, USA
[4]Harvard Medical School, Boston, MA, USA
[5]Biological and Biomedical Sciences Program, Harvard Medical School, Boston, MA, USA
[6]Biostatistics Branch, Division of Cancer Epidemiology and Genetics, National Cancer Institute, Bethesda, MD, 20892, USA
[7]Division of Oncology, Department of Clinical Sciences, Faculty of Medicine, Lund University, Lund, 22185, Sweden
[8]Lund University Cancer Center, Lund, 22185, Sweden
[9]Protein Characterization Laboratory, Frederick National Laboratory for Cancer Research, Leidos Biomedical Research Inc, Frederick, MD, USA
[10]Laboratory of Genomic Susceptibility, Division of Cancer Epidemiology and Genetics, National Cancer Institute, Bethesda, MD, 20892, USA
[11]Genome Modification Core, Frederick National Laboratory for Cancer Research, Frederick, MD, USA
[12]Institute of Basic Medical Sciences, Chinese Academy of Medical Sciences, Beijing, 100005, China
[13]Neuroscience Graduate Program, University of Michigan, Ann Arbor, MI, USA
[14]Integrative Tumor Epidemiology Branch, Division of Cancer Epidemiology and Genetics, National Cancer Institute, Bethesda, MD, 20892, USA
[15]Leeds Institute of Medical Research, School of Medicine, University of Leeds, Leeds, UK
[16]Leeds Institute for Data Analytics, University of Leeds, Leeds, UK
[17]Population Health Sciences Institute, Faculty of Medical Sciences, Newcastle University and NIHR Biomedical Research Centre, Newcastle upon Tyne, UK
[18]NIHR Leeds Biomedical Research Centre, Leeds Teaching Hospitals NHS Trust, Leeds, UK
[19]Population Health Department, QIMR Berghofer Medical Research Institute, Herston, QLD, Australia
[20]School of Biomedical Sciences, Faculty of Health, Queensland University of Technology, Brisbane, QLD, Australia
[21]School of Biomedical Sciences, University of Queensland, Brisbane, QLD, Australia

[*] authors contributed equally
[#] corresponding author; kevin.brown3@nih.gov

The authors declare no potential conflicts of interest

Abstract

Genome-wide association studies identified a melanoma- and nevus count-associated locus on chromosome band 9q34.13. Fine-mapping and melanocyte expression data collectively suggest two potential causal genes with opposite association with risk: higher levels of Rap guanine nucleotide exchange factor 1 (*RAPGEF1*) and lower levels of uridine-cytidine kinase 1 (*UCK1*). Colocalization analyses and conditional TWAS suggest multiple causal *cis*-regulatory sequence variants in partial linkage disequilibrium (LD) to each other. Melanocyte capture-HiC and CRISPR-inhibition demonstrated regulatory interactions between fine-mapped variants and the *RAPGEF1* and *UCK1* promoters. Focusing on *RAPGEF1*, we demonstrate *RAPGEF1* expression promotes melanocyte growth and drives malignant transformation of human immortalized melanocytes. Following treatment with human EGF, *RAPGEF1* overexpression activated both RAP1 and RAS. Further, we show *RAPGEF1* expression is significantly enriched in melanomas lacking strongly activating RAS-MAPK mutations, suggesting that *RAPGEF1* may promote oncogenic RAS-MAPK signaling in melanomas. Furthermore, in these tumors, we provide preliminary evidence to support the prognostic relevance of *RAPGEF1* expression in patients lacking *RAS* or *BRAF* mutations. Together with other recent studies, these data suggest that germline variation influencing RAS activation may play a key role in nevus development and melanoma risk.

Introduction

Meta-analysis of genome-wide association studies (GWAS) for melanoma have identified 54 loci and 68 independent signals associated with melanoma risk [1]. Despite the success in identifying loci, the causal sequence variants and specific genes at these loci that influence risk and melanoma development remain to be established. Linkage disequilibrium (LD) typically results in numerous risk-associated variants, complicating efforts to identify causal variants. Further, most fine-mapped variants at complex trait loci identified by GWAS are not protein coding; instead most causal variants alter *cis*-regulatory activity of regulatory sequences including enhancers and promoters [2, 3]. Given that enhancers can act at distances of 1Mb or more [4, 5], numerous genes near risk-associated loci may be plausible causal candidates.

Identifying causal sequence variants and their gene targets is important to understanding potentially unappreciated key processes underlying risk, tumor development, and or tumor progression. Of known risk loci, the majority are also associated with heritable melanoma risk-associated traits [1], including hair, skin or eye color [1, 6], telomere length [1, 7-9], and number of melanocytic nevi [1, 10-12]. While these pleiotropic associations can provide clues to the likely causal genes at melanoma risk loci, establishing causal genes for most loci remains a challenge.

We and others have previously generated multiple genome- or GWAS-scale genomic, transcriptomic, epigenomic, chromatin conformation, and functional screening datasets in melanocytic cells or tissues relevant to melanoma risk [13-24]. Here we layer analyses of these datasets and characterize a melanoma risk and nevus count locus on chromosome band 9q34.13 [1] near the 3′-end of RAP guanine nucleotide exchange factor 1 (*RAPGEF1*, also known as C3G) and establish the *RAPGEF1* gene as one of two potential causal candidate genes at this locus. We demonstrate that *RAPGEF1* expression promotes melanocyte proliferation, increases colony formation in immortalized melanocytes, and leads to both RAP1 and RAS activation. Finally, we demonstrate higher expression of *RAPGEF1* in melanoma tumors lacking RAS-pathway driver mutations consistently across multiple tumor sequencing datasets. These data suggest that germline modulation of RAS activity may play a key role in both nevus and melanoma development.

Methods

Genetic fine-mapping at the melanoma risk locus on chromosome band 9q34.13

We fine-mapped the melanoma risk locus on chromosome band 9q34.13 (a ±500 Kb window surrounding rs3780269) to identify potential causal variants. We applied multiple Bayesian fine-mapping methods including SuSiE (Sum of Single Effects) [25, 26], DAP-G [27, 28] (Deterministic Approximation of the Posteriors), and RSparsePro [29], which is robust to mismatching LD between the GWAS and the LD-reference panels. We used default parameters for each method. The min_abs_corr parameter was set to 0 for SuSiE. Melanoma GWAS Z-score values for each variant were from the fixed-effect inverse variance weighted meta-analysis of the full set of confirmed and self-reported melanoma cases and control, as described previously by Landi and colleagues [1]. We used a pre-computed LD matrix of 5,000 UK Biobank individuals as described previously [1]. While we allowed for a maximum of five credible sets during fine-mapping, we only retained individual credible sets where the cumulative posterior inclusion probability was > 0.85, and retained all variants in the credible set where the individual variant posterior inclusion probability was > 0.005. To inclusively fine-map variants, we also independently selected any variants with log likelihood ratio (LLR 1:1000) relative to the GWAS lead variant rs3780269. Finally, to assess variants that were not successfully genotyped or imputed in the GWAS (including notably insertion/deletion variants that were not a part of the Haplotype Reference Consortium imputation panel), we included any such variants that had an LD $r^2 > 0.8$ (1000 Genomes Project, Phase 3, Version 5, EUR population) [30] with rs3780269 as identified by the LDlinkR package [31-33].

To further assess the possibility of other potential independent signals in the region, we conditioned on the lead GWAS variant (rs3780269) using the Genome-wide Complex Trait Analysis (GCTA, v1.94.1) [34] COnditional and JOint association (COJO) module [35], using default settings, a genomic window of ±1 Mb from the lead variant, and the UKBB LD matrix described above.

Annotation of fine-mapped variants

We assessed all fine-mapped variants at this locus for overlap with melanocytic regulatory elements (defined by chromatin states, or accessibility) using the BedtoolsR package (intersect function) [36, 37] and epigenomic datasets from melanocytes and melanoma cell line models. We classified genomic regions as enhancers or promoters using the Roadmap project chromHMM data from two primary melanocyte cultures [17, 20]. Using this data, enhancers were defined using the following chromHMM states from all chromHMM tracks (primary: Enh, EnhG, EnhBiv; auxiliary: EnhG1, EnhG2, EnhA1, EnhA2, EnhWk, EnhBiv; and imputed: TxEnh5, TxEnh3, TxEnhW, EnhA1, EnhA2, EnhAF, EnhW1, EnhW2, EnhAc). Melanoma-specific enhancer annotations included 4_EnhA, 5_EnhM, 6_EnhW, 7_TxEnhM, 7_TxEnhW, and 9_TxWkEnhW, from a tumorigenic melanoma cell model [21]. Promoter states were defined in melanocytes from imputed ChromHMM as PromU, PromD1, PromD2, TssA, PromP, PromBiv, and Tx_Reg; and in melanoma cells as 1_TssA, 2_PromWkD, and 3_TssWkP. We analyzed our previously generated ATAC-seq data from five independent melanocyte cultures [22], along with publicly available omni-ATAC-seq data from nine melanoma cell lines derived from patient biopsies [19]. Any region annotated as enhancer or promoter or that overlapped ATAC-peak in either melanocyte or melanoma cells was considered *cis*-regulatory.

Allele-specific transcriptional activity of these variants was previously assessed using Massively Parallel Reporter Assays (MPRA) in immortalized primary melanocytes and UACC903 melanoma cells [23]. All fine-mapped variants for the melanoma risk signal were included in the MPRA library design, however one failed data QC and was subsequently excluded from analysis. Allelic impacts on transcriptional activity were assessed using a linear regression model, accounting for strand and transfection batch as covariates. A scrambled 145-bp sequence was used as a negative control and as a baseline to assess relative enhancer activity of specific regions surrounding fine-mapped variants. Allele-specific differences for each variant were tested relative to scrambled controls. Multiple hypothesis testing was corrected using Benjamini-Hochberg false discovery rate.

We assessed the impact of fine-mapped variants on the protein-coding sequence Variant effect predictor tool (https://grch37.ensembl.org/Homo_sapiens/Tools/VEP) [38] using GENCODE version 19 protein-coding transcripts.

155

156 *Cell culture*

157 Frozen aliquots of melanocytes isolated from foreskin of healthy newborn males, mainly of
158 European descent, were obtained from the Specialized Programs of Research Excellence
159 (SPORE) in Skin Cancer Specimen Resource Core at Yale University following an established
160 protocol [39]. Melanocytes were grown in Dermal Cell Basal Medium (American Type
161 Culture Collection/ATCC PCS-200-030) supplemented with Melanocyte Growth Kit (ATCC
162 PCS-200-041) and 1% amphotericin B/penicillin/streptomycin (120-096-711, Quality
163 Biological) at 37°C with 5% CO_2. Immortalized C283T [18] melanocytes as well as C283T cells
164 stably expressing dCas9-KRAB [22] were generated as previously described and grown in
165 identical conditions to primary melanocytes. All cells tested negative for mycoplasma
166 contamination via MycoAlert PLUS Mycoplasma Detection Kit (LT07-710, Lonza).

167

168 *Assessing micro-RNA binding for variant overlapping RAPGEF1 3'-UTR region*

169 To assess whether melanoma GWAS risk variant rs3739497, which resides in the *RAPGEF1*
170 3 untranslated region (UTR), is involved in potential post-transcriptional regulation of
171 *RAPGEF1* through micro-RNAs (miRNAs), we assessed predicted miRNA binding sites near
172 this variant. We queried several databases, including TargetScan [40], miRTarBase [41],
173 miRDB [42, 43], and mirCode [44]. Binding sites that overlapped or were located within ±50
174 nucleotides of the variant position were considered candidate variant-dependent miRNA
175 sites. Finally, to explore post-transcriptional regulation via sequence elements other than
176 miRNAs, we queried the 3'UTR variant region against the AREsite database [45] that
177 provides a genome-wide catalogue of AU-rich elements.

178

179 *Small RNA sequencing data from primary melanocytes and melanomas*

180 To assess small RNA levels in primary human melanocytes (n=106), total RNA, including
181 microRNA (miRNA), was purified using Qiagen miRNeasy kit (#217004). Briefly, cells were
182 lyzed in Trizol and heated at 65C followed by chloroform extraction. The aqueous phase was
183 further purified using a miRNeasy column following manufacturer's instruction. miRNA
184 sequencing libraries were constructed using NEB Next Small RNA Library Prep kit (E7330s)

185 and the sequencing was performed on HiSeq2500. All samples show the proportion of Q30
186 or higher bases of at least 93%. 28-79 million reads were achieved for each sample with
187 overall alignment percentage between 67-85%. Sequencing reads were processed using the
188 mirMaster pipeline [46]. Quality control stage processing steps included removal of 3′
189 adapter sequences (AGATCGGAAGAGCACACGTCTGAACTCCAGTCAC), trimming of low-
190 quality bases, and retention of reads that exceeded the default minimum length thresholds.
191 Reads were then aligned to the human genome (GRCh38) using Bowtie [47], allowing up to
192 five genomic alignments per read. miRNAs were quantified by aligning sequencing reads
193 against the mature and precursor miRNA reference sequences from miRBase v22.1 [48-53].
194 Alignments permitted up to one mismatch. Expression values were normalized across
195 samples using quantile normalization. For each miRNA, percentile rank of expression across
196 the dataset was calculated based on median expression values.

197 *RAPGEF1* mRNA expression levels were available from the bulk RNA-seq data we previously
198 simultaneously generated from the same 106 melanocyte cultures [13]. The correlation of
199 *RAPGEF1* mRNA expression levels with candidate miRNAs was measured using Spearman's
200 rank correlation.

201 Expression levels of micro-RNAs in TCGA melanoma samples [14] were accessed through
202 FirebrowseR (https://github.com/mxxdxxx/FirebrowseR).

203

204 *Quantitative Trait Locus (QTL) analysis of melanocytic cells*
205 We assessed FDR significant QTL signals near the GWAS risk locus using previously-published
206 melanocyte and melanoma datasets [9, 12]. Melanocyte expression QTL (eQTL), splice QTL
207 (sQTL), and methylation QTL (meQTL) datasets were generated from 106 primary
208 melanocyte cultures derived from individuals of European descent. Methylation probes
209 from meQTL data were assigned to genes based on CpG location within 1.5 kb of the TSS,
210 5′-UTR, 1st exon, gene body, or 3′-UTR of a gene. Tumor eQTL data were derived from
211 TCGA melanoma primary tumors as a part of the PancanQTLv2.0 eQTL study; only data from
212 nominally significant SNP-gene pairs (P<0.01) were made available [79]
213 (https://hanlaboratory.com/PancanQTLv2/).

214 GWAS colocalization using the melanocyte eQTL dataset was performed using the SuSiE +
215 Coloc [54] and SharePro tools [55]. SuSiE + Coloc performs fine-mapping of GWAS and QTL
216 signals via SuSiE, followed by colocalization via the Coloc tool. SharePro leverages linkage
217 disequilibrium (LD) to cluster correlated variants into effect groups, followed by
218 colocalization. GWAS summary data, and the *RAPGEF1* and *UCK1* melanocyte eQTL
219 summary data (± 500 Kb around the lead variant) were used as input for this analysis.
220 Default parameters were used except the sigma parameter, which represents the prior
221 probability of colocalization between traits. Since the region being assessed harbors
222 multiple GWAS/QTL signals with complex LD, we provide results using multiple sigma values,
223 ranging from most stringent (1×10^{-5}) to less stringent (1×10^{-4}, 1×10^{-3}). However given that
224 relaxing this value from the default of 1×10^{-5} increases the potential for false positive
225 findings, we formally tested colocalization using this default value. Colocalization probability
226 > 0.8 was considered strong evidence supporting colocalization, while a colocalization
227 probability < 0.2 was considered evidence against colocalization [55].

228 We also used these QTL datasets to perform transcriptome (melanocyte and TCGA
229 melanoma tumors) and methylome-wide (melanocyte) association studies (TWAS/MWAS).
230 To identify conditionally independent loci, we performed conditional TWAS analysis using
231 the FUSION tool [56].

232

233 *Capture-HiC assay for linking risk variants to target genes*

234 As described previously [22], we performed melanoma GWAS-region focused capture Hi-C
235 assays in primary human melanocytes to facilitate variant-to-gene mapping across all 68
236 melanoma genome-wide significant signals. Capture probes were designed by Arima
237 Genomics (San Diego, CA) using 2x tiling with least stringent masking and XTHSBoosting,
238 resulting in an Agilent SureSelect library (Santa Clara, CA) targeting all restriction fragments
239 generated by DpnII and MboI (recognition sites: GATC, GANTC) within each association
240 interval. We generated 15 capture Hi-C libraries from five independent primary melanocyte
241 cultures (C56, C140, C205, C24, and C27), with three technical replicates prepared per
242 culture. Barcoded libraries were pooled and sequenced on an Illumina NovaSeq platform
243 across one SP and one S1 flow cell, yielding ~5.7 billion 150 bp paired-end reads in total.

244 Sequencing reads were processed using the HiCUP pipeline [57] with alignment to the hg19
245 reference genome via Bowtie2 [58]. Technical replicates from each melanocyte culture were
246 combined prior to downstream analyses. Chromatin interactions were detected using the
247 CHiCAGO pipeline (v1.16.0) [59] at both individual restriction fragment-level and aggregated
248 four-fragment resolution, as previously described [22]. Interactions with CHiCAGO scores >5
249 were considered high-confidence visualized on the WashU [60, 61] and UCSC genome
250 browsers [62-66]. To mitigate cross-linking variability and restriction fragment boundary
251 effects, we expanded each fine-mapped variant into a ±500 bp window and evaluated
252 interactions from both the variant-overlapping and adjacent fragments. Genes were
253 nominated as candidate targets if a chromatin interaction was observed from a variant-
254 harboring (or adjacent) restriction fragment to the target gene promoter. To map *cis*-
255 regulatory targets of enhancer-promoter interactions, candidate genes initially nominated
256 based solely on physical chromatin interactions with fine-mapped variants were further
257 refined by evaluating whether these variants overlapped melanocytic regulatory regions.

258

259 *CRISPRi validation of regulation of RAPGEF1 and UCK1 transcription*

260 To validate regulatory interactions from risk variants to target genes, we performed CRISPR
261 interference (CRISPRi) assays in the immortalized human melanocyte cell line C283T stably
262 expressing dCas9-KRAB [22]. Briefly, C283T cells were infected with a lentiviral vector
263 pLX_311-KRAB-dCas9 (gift from John Doench, William Hahn, and David Root; Addgene
264 plasmid # 96918; http://n2t.net/addgene:96918; RRID: Addgene_96918) followed by
265 monoclonal cell selection. We confirmed stable expression and functional activity of dCas9-
266 KRAB in the clone used for CRISPRi.

267 Three different guide RNAs (gRNAs) were designed to target the genomic regions flanking
268 each variant site. The gRNA sequences were located ±50bps from the variant
269 (**Supplementary Table 1**). We used two non-targeting gRNAs (NTC1, NTC2) as controls.
270 gRNAs were ligated into the lentiviral vector pXPR-050 (gift from John Doench and David
271 Root, Addgene plasmid #96925; RRID: Addgene_96925). C283T immortalized melanocytes
272 [18] were infected with lentiviral particles encoding gRNA, and at 24h, 1.5 µg/mL of
273 puromycin was added for selection. After two days of puromycin selection, puromycin was
274 removed, and cells were harvested for RNA collection on the same day or one day after

275 puromycin removal. Total RNA was isolated with RNeasy Mini Kit (Qiagen) and cDNA was
276 generated with SuperScript IV VILO Master Mix (Thermo Scientific). Multiple infections were
277 performed with total ten biological replicates for each gRNA against the 3 different variants.
278 mRNA levels of either *RAPGEF1* or *UCK1* were measured by TaqMan assay (Thermo
279 Scientific; **Supplementary Table 1**) and normalized to *GAPDH* levels. qPCR triplicates
280 (technical replicates) were averaged and subsequently considered as a single data point.
281 Average $2^{\wedge(\text{delta-Ct})}$ values for NTC1 and NTC2 were used for statistical comparisons to other
282 gRNAs, data in tables and graphs are represented as fold-change relative to the average of
283 NTC1 and NTC2. The statistical analysis was performed using a paired two-tailed t-test
284 comparing $2^{\wedge(\text{delta-Ct})}$ values of individual guides to the average $2^{\wedge(\text{delta-Ct})}$ of NTC1/NTC2.

285

286 *Knock-down of RAPGEF1 and UCK1 expression by shRNA and qRT-PCR quantification of gene*
287 *expression*
288 Pre-designed shRNAs against human *RAPGEF1* and *UCK1* genes were purchased from Sigma
289 (TRCN0000048129 and TRCN0000048130 for *RAPGEF1*, TRCN0000037763 and
290 TRCN0000199254 for *UCK1*; **Supplementary Table 1**) and expressed in lentiviral vector
291 backbone (pLKO). After viral infection and puromycin selection, total RNA was isolated with
292 the RNeasy Mini Kit (Qiagen) and cDNA was generated with SuperScript IV VILO Master Mix
293 (Thermo Scientific). Transcript levels were measured using TaqMan qPCR assays purchased
294 from Thermo Scientific. *RAPGEF1* and *UCK1* transcript levels were normalized to the levels
295 of *GAPDH*, and PCR triplicates were averaged and considered as one data point.

296

297 *Overexpression of RAPGEF1 in human melanocyte culture*
298 *RAPGEF1* was cloned from a cDNA construct (OHS5893-202500127, ORFeome Collab,
299 Horizon Discovery) into pLX304 (a gift from David Root, Addgene plasmid # 25890;
300 http://n2t.net/addgene:25890) or pCW57.1 (a gift from David Root, Addgene plasmid #
301 41393; http://n2t.net/addgene:41393) lentiviral vectors. This clone is the isoform most
302 strongly expressed across neonatal melanocytes [13]. pCW57.1 contains a doxycycline
303 inducible promoter. Lentiviral vectors were co-transfected into HEK293 cells with the
304 pSPAX2, pMD2-G, and pCAG4-RTR2 packaging vectors. Virus was collected two days after

305 transfection and concentrated by Vivaspin Concentrators (76409-072, VWR). Cells were
306 incubated with virus for 24 h, followed by selection with blasticidin (5-10ug/ml) or
307 puromycin (1–2 µg/ml) for 2–4 days. For pCW57.1-RAPGEF1 infected cells, RAPGEF1
308 expression was induced by 0.2ug/ml doxycycline in melanocyte culture.

309

310 *Gene-based CRISPR-Cas9 knockout screen*

311 A gene-based pooled CRISPR-Cas9 cell proliferation knockout screen was previously
312 performed in an immortalized human melanocyte culture, C283T, as described by Xu and
313 colleagues [14]. Briefly, we designed 3,052 gRNAs covering a set of 288 genes, as well as
314 ~200 non-targeting gRNAs. The 288 genes focused primarily on gene candidates from
315 genome-wide significant melanoma GWAS loci. DNA samples were collected from sgRNA
316 infected cells at different times after infection and gRNAs were sequenced and normalized
317 to counts of the integrated gRNA sequence from cells collected prior to Cas9 expression.
318 Prioritized gene hits critical for cell growth and/or survival were called and ranked by using
319 MAGeCK.

320

321 *Cell proliferation assays*

322 Cell proliferation was assayed using a BrdU flow kit (BD Pharmingen) according to the
323 manufacturer's protocol. Briefly, cells were labeled with 10 µM BrdU for 1-3 hours before
324 they were fixed, permeabilized, and subjected to DNase I treatment. Cells were then stained
325 with FITC-conjugated antibody to BrdU and 7-AAD, followed by flow cytometry analysis
326 using an AttuneNxT Cytometer (Thermo Scientific). For crystal violet staining, cells were
327 seeded at equal numbers after infection and drug selection and were stained with crystal
328 violet at different days after seeding. Crystal Violet was solubilized by methanol for
329 quantification as absorbance at 560nm.

330

331 *Immunoblotting*

332 For immunoblot analysis, total cell lysates were generated with RIPA buffer (Thermo
333 Scientific) and subjected to water bath sonication. Samples were resolved by 4–12% Bis-Tris

334 ready gel (Invitrogen) electrophoresis. The primary antibodies used were mouse antibody to
335 RAPGEF1 (MA5-26281, ThermoScientific), mouse antibody to RAS (05-516, Sigma), rabbit
336 antibody to RAP1 (ab181858, Abcam), mouse antibody to phospho-ERK(9106S, Cell Signaling
337 Technology), mouse antibody to Pan-AKT (2920s, Cell Signaling Technology), rabbit antibody
338 to total ERK(4695s, Cell Signaling Technology), rabbit antibody to Phospho-AKT(4060s, Cell
339 Signaling Technology), and mouse antibody to β-actin (A5316, Sigma).

340

341 *Colony formation assays*

342 Anchorage-independent growth was assayed with p'mel/BRAF^{V600E} cells (provided by H.
343 Widlund, Dana-Farber Cancer Institute). Briefly, 5,000 cells were mixed in HAMF12 medium
344 supplemented with 10% FBS containing 0.4% SeaKem LE agarose (Lonza) and plated on top
345 of a bottom layer with 0.65% agarose prepared in the same HAMF12 medium in a six-well
346 plate. After agarose is solidified, each well was covered with 0.5 ml of feeding medium,
347 which was refreshed twice a week. Colonies were counted and imaged 4-6 weeks after
348 seeding using Lionheart (Agilent) with total magnification of 4x. Colonies were counted from
349 six wells for each condition, and significant differences between samples were assessed by
350 unpaired two-tailed *t*-test assuming equal variance.

351

352 *Zebrafish Melanoma Generation and Analysis*

353 Zebrafish melanomas were generated by overexpressing human RAPGEF1 (cloned from a
354 cDNA construct, OHS5893-202500127, ORFeome Collab, Horizon Discovery; same *RAPGEF1*
355 isoform expressed in human melanocyte experiments) or an empty control vector (MCS) in
356 transformed melanocytes using the miniCoopR system [67]. This system involves injection of
357 a Tol2-based miniCoopR vector into the *Tg(mitfa:BRAF^{V600E}); p53(lf); mitfa(lf)* zebrafish
358 strain, where it rescues melanocyte development and simultaneously drives expression of a
359 gene of interest under the *mitfa* promoter. To visualize melanocytes, we co-injected
360 *mitfa:Cas9*, CRISPR gRNAs targeting *tyrosinase* (to block pigmentation), and *mitfa:mCherry*.
361 As melanocyte rescue is mosaic in this system, we screened these cohorts for fish that had
362 *mitfa:mCherry* melanocyte expression in either the RAPGEF1 cohort (n=35), or the MCS
363 control cohort (n=48). These cohorts were comprised of two separate clutches per condition

364 and were genotyped to confirm RAPGEF1 expression status. Starting at 13 weeks post-
365 fertilization, we monitored fish for precursor lesions—termed "cancer precursor zones"
366 (CPZ)—defined as patches of merged *mitfa:mCherry*-high melanocytes exceeding
367 established size and fluorescence thresholds. Screening continued every few weeks until 46
368 weeks post-fertilization. Kaplan-Meier survival analysis and log-rank (Mantel-Cox) tests
369 showed no significant differences in CPZ onset (p=0.1119) or tumor onset (p=0.211)
370 between groups. Tumor anatomical distribution did not differ substantially between groups.

371 RAPGEF1 functions upstream of BRAF in the MAPK pathway, and since our primary zebrafish
372 tumor model overexpresses oncogenic *BRAF*^{V600E}, this could obscure a role for RAPGEF1 or
373 represent a different biological context to that seen *in vitro*. To assess this, we used the
374 MAZERATI system (Modeling Approach in Zebrafish for Rapid Tumor Initiation) [68] to
375 generate zebrafish cohorts where rescued melanocytes expressed either *BRAFV600E/p53(lf)*
376 or *RAPGEF1/p53(lf)*. In this system, *mitfa:BRAFV600E* and *p53(lf)* mutations are not stably
377 expressed in the zebrafish strain background, but are delivered via plasmid injection at the
378 one-cell stage, allowing us to test whether RAPGEF1 alone can drive tumor initiation in the
379 absence of an activating BRAF mutation. While the *BRAFV600E/p53(lf)* cohort developed
380 tumors at the expected rate, *RAPGEF1/p53(lf)*– fish failed to develop precursor lesions or
381 tumors.

382

383 *RAP1 and RAS activation assay*

384 RAP1 activation was measured using the RAP1 activation assay kit from Abcam (ab212011)
385 and RAS activation was measured using GST-fusion Raf-1 RBD beads (Sigma, #14863) or RAF-
386 RBD Protein GST Beads (RF02-A, Cytoskeleton). Cells were grown in supplement-free ATCC
387 medium for 24 hours before treated with 50ng/ml human EGF protein (R&D, Cat# 236-EG-
388 200) at the indicated time. Whole cell extract was taken to be pulled down by the Raf-RBD
389 beads for RAS activation assay or by the RalGDA RBD beads from the Abcam kit for
390 measuring RAP1 activation. Beads were then lysed in SDS loading buffer, resolved by 4–12%
391 Bis-Tris ready gel (Invitrogen) electrophoresis, and blot with RAS (Sigma) or RAP1 (Abcam)
392 antibody. Only the active GTP-bound form of RAS or RAP1 can be pulled down by the beads
393 and the intensity of RAS or RAP1 activation was determined by comparing the pulled-down
394 signal with that from the whole cell extract.

Assessing RAS-MAPK alterations across multiple melanoma cohorts

We assessed *RAPGEF1* expression association with activating mutations in RAS-MAPK signaling pathway in melanoma tumors. We analyzed cutaneous melanoma tumors across six cohorts: TCGA n=363 [14], Leeds n=503 [69-71], Lund n=146 [72], Liu n=84 [73], Van Allen n=38 [74], Riaz n=39 [75] (**Supplementary Tables 2-8**). Briefly, the Leeds, Lund, and TCGA cohorts included very few samples treated with immunotherapy (TCGA n=23 [76]; Leeds n=12 [70]; and Lund n=4 [72]), while the other three cohorts consisted of patients treated with immunotherapy following tumor collection. Our sample inclusion criteria required melanoma samples that had both mutation and gene expression data available across the cohorts. Cohort details are provided in the **Supplementary Materials**.

Assessing RAPGEF1 expression association with RAS-pathway

We tested several models classifying RAS-pathway wild-type and mutant tumors, focusing initially on the most commonly-mutated oncogenic driver genes and subsequently adding in less-commonly altered genes. Specifically, within the Leeds sample set (n = 503 total), only specific mutations in *BRAF* (V600|K601) and *NRAS* (Q61|G12|G13) were assessed in a subset of the tumors (n=234), while for the remaining a full set of putative MAPK driver mutations [77] were assessable from sequencing data, so our initial model (Model 1) defined the mutant subgroup as those samples with these specific *BRAF* (V600|K601) and *NRAS* (Q61|G12|G13) hotspot mutations. Additional models were as follows: Model 2 mutant group, any driver mutation in *BRAF* or *NRAS*; Model 3 mutant group, any driver mutation in *BRAF*, *NRAS*, *KRAS*, or *HRAS*; Model 4 mutant group, any driver mutation in *BRAF*, *NRAS*, *KRAS*, *HRAS*, or *NF1* ("triple wild-type); and Model 5, any putative driver mutation in the 44 genes defined from the TCGA Pan-Cancer analysis [77] (**Supplementary Table 9**). Outside of the Leeds dataset, all cohorts had full mutation information for *BRAF*, *NRAS*, *KRAS*, *HRAS*, and *NF1*. As described above, Leeds and Lund cohorts had targeted sequencing of select cancer-related genes and were not fully assessed for all genes included in Model 5. In this case for Model 5, we classified wild-type and mutant subgroups based on the available gene sequencing data from each dataset. Methods for annotating individual

425 mutations as drivers are described in the **Supplementary Material**. We assessed an
426 association of *RAPGEF1* levels with RAS-MAPK wild-type and mutant subgroups using a
427 linear regression model, adjusting for age, sex, tumor purity, and tumor stage when
428 available.

429

430 *Survival analysis*

431 We conducted survival analyses across multiple melanoma cohorts using the Cox
432 proportional hazards models to assess the association between *RAPGEF1* expression and
433 patient outcomes in tumors wild-type for *BRAF* (V600|K601) or *NRAS* (Q61|G12|G13)
434 hotspot mutations. For each cohort, *RAPGEF1* expression was dichotomized into high- and
435 low-expression groups based on the median expression value of the full dataset.
436 Associations between *RAPGEF1* expression and survival were then evaluated within the
437 wild-type tumor subgroup using the Cox models. To ensure comparability across datasets,
438 all survival times were uniformly converted to days. We performed melanoma-specific
439 survival in the TCGA, Leeds, and Lund cohorts, and overall survival in the Liu, Van Allen, and
440 Riaz cohorts as they lacked melanoma-specific death data. Because stage I tumors were
441 profiled exclusively in the Leeds cohort and are associated with a high survival rate (93-97%)
442 [78], we excluded these tumors from the survival analysis to ensure comparability between
443 the Leeds cohort and other melanoma cohorts, which predominantly included more
444 advanced-stage tumors. For these analyses, we adjusted for covariates specific to each
445 cohort as follows: TCGA: Age, Tumor site; Leeds: Age; Lund: Age; Liu: Cosmic aging; Van
446 Allen: Age. Across all cohorts, the WT tumor subgroup included only a small number of
447 samples, and when the number of events is low relative to the number of covariates, the
448 Cox model can encounter monotone likelihood issues, resulting in extremely large or
449 unstable coefficient estimates. To address this, we applied Firth's correction.

450

451 *Meta-analysis of tumor data*

452 We performed meta-analysis of the *RAPGEF1* expression association with RAS-MAPK
453 subgroups, as well as the association of *RAPGEF1* expression with survival across the
454 analyzed melanoma cohorts as follows: Let be the z-score for cohort . Let $^{+}$ be the number

455 of subjects with the mutation and $^{-}$ be the number of subjects of wild type, then the

456 effective sample size $= \frac{+-}{++-}$. We choose weights $= \sqrt{/\sum_{=1}^{5}}$ and perform meta-analysis

457 as $= \sum_{=1}^{5}$. One can show that $\sim(0,1)$ under $_{0}$ and has optimal statistical power assuming

458 equal effect sizes (after normalization).

459

460 **Results**

461 *Fine-mapping of the 9q34.13 melanoma risk signal*

462 In order to functionally characterize the melanoma risk locus on chromosome band 9q34.13,

463 which is also associated with nevus count, but not hair color, tanning ability, or telomere

464 length [1], we first assessed whether the locus harbors a single or multiple risk signals.

465 Conditional GWAS analysis using the lead variant at this locus (rs3780269, P_{GWAS}=1.92 x 10^{-8},

466 rs3780269-G OR=0.94) revealed no evidence of a secondary signal within +/- 1Mb of the

467 main GWAS association signal (**Supplementary Table 10-11**, **Supplementary Figure 1A**).

468 Multiple Bayesian fine-mapping methods (SuSiE, DAP-G, and RSparsePro) [25-29] similarly

469 converged on a single and similar credible causal set of variants (CCVs; **Supplementary**

470 **Table 12**).

471 To facilitate variant-to-gene mapping, we defined a credible causal set by taking the union

472 of CCVs identified using Bayesian fine-mapping approaches. Within this set, the GWAS lead

473 variant (rs3780269) was consistently assigned the highest posterior probability of being

474 causal across methods (DAP-G PIP = 0.52, RSparsePro PIP = 0.58, SuSiE PIP = 0.55). We also

475 included as CCVs variants identified by fine-mapping directly from GWAS summary statistics

476 by assessing log-likelihood ratio (LLR) relative to the lead variant. Finally, to account for

477 additional variants not genotyped or imputed in the GWAS, we performed LD-based fine-

478 mapping (r^2 > 0.8 with the lead variant). These methods collectively identified 14 potential

479 causal variants (**Figure 1A, Supplementary Table 12**).

480 None of these variants mapped to protein-coding sequence or canonical splice junctions

481 (**Supplementary Table 13**), nor was there a significant or colocalizing splice QTL (sQTL) for

482 rs3780269 (see **Supplementary Material**). One fine-mapped variant, rs3739497 (P_{GWAS} = 1.9

483 × 10^{-6}; OR = 0.95; risk allele = A; protective allele = G; r^2 to GWAS lead = 0.88), is located in

484 binding site for two microRNAs (miRNAs; *miR-124-3p* and *miR-506-3p*) in the 3

485 untranslated region (UTR) of *RAPGEF1*, however we found no evidence that levels of
486 *RAPGEF1* were correlated with either in melanocytes, making it unlikely this variant impacts
487 either miRNA binding or *RAPGEF1* levels (see **Supplementary Material**).

488 *The 9q34.13 melanoma risk region physically interacts with and regulates RAPGEF1 and*
489 *UCK1*

490 Several melanoma credible set variants overlap active enhancer or accessible chromatin
491 regions in human melanocytes or melanoma cell models (**Figure 1B, Supplementary Table**
492 **14**), while the lead variant is located within a region broadly annotated as an enhancer
493 across multiple cell types (ENCODE *cis*-regulatory element EH38E2732514)[79], suggesting a
494 *cis*-regulatory function. Consistent with this annotation, previous massively parallel reporter
495 assays (MPRA) of fine-mapped risk variants [23] showed the regions surrounding several
496 had significantly different transcriptional activity compared to scrambled DNA sequences in
497 melanocytes and melanoma cells (scramble vs alt comparisons in **Supplementary Table 15**),
498 indicating enhancer and/or repressive function (**Supplementary Figure 2**).

499 Capture-HiC-based variant-to-gene mapping [22] of the full region of association in primary
500 melanocytes identified chromatin interactions between enhancers harboring fine-mapped
501 variants (**Supplementary Table 14**) and the promoters of *RAPGEF1 and UCK1* (**Figure 1A**;
502 **Supplementary Table 16**), as well as to *NTNG2* (which is lowly-expressed in melanocytes
503 and melanoma). CRISPR-inhibition (CRISPRi) of regions surrounding select variants
504 interacting with *RAPGEF1* and *UCK1* promoters (**Figure 1B**) in immortalized melanocytes
505 confirmed a *cis*-regulatory effect of the region surrounding the GWAS lead variant
506 (rs3780269) for both *RAPGEF1* (2/3 guide RNAs; 0.85–0.88 fold relative to non-targeting
507 controls, $P = 0.0031$ and $P = 0.0018$ respectively; paired Student's t-test) and *UCK1* (2/3
508 gRNAs 0.78–0.82 fold, $P = 0.0025$ and $P = 0.0021$ respectively; paired Student's t-test), as
509 well as rs3818580 for *UCK1* (2/3 guides; $P = 0.025$ and $P = 0.031$) (**Figure 1C**). However,
510 melanocyte and melanoma MPRA data for credible set variants [23] did not find variants
511 with significant allelic differences in transcriptional activity (ref versus alt columns in
512 **Supplementary Table 15**), so while elements in this region regulate both genes, these data
513 do not implicate a specific variant.

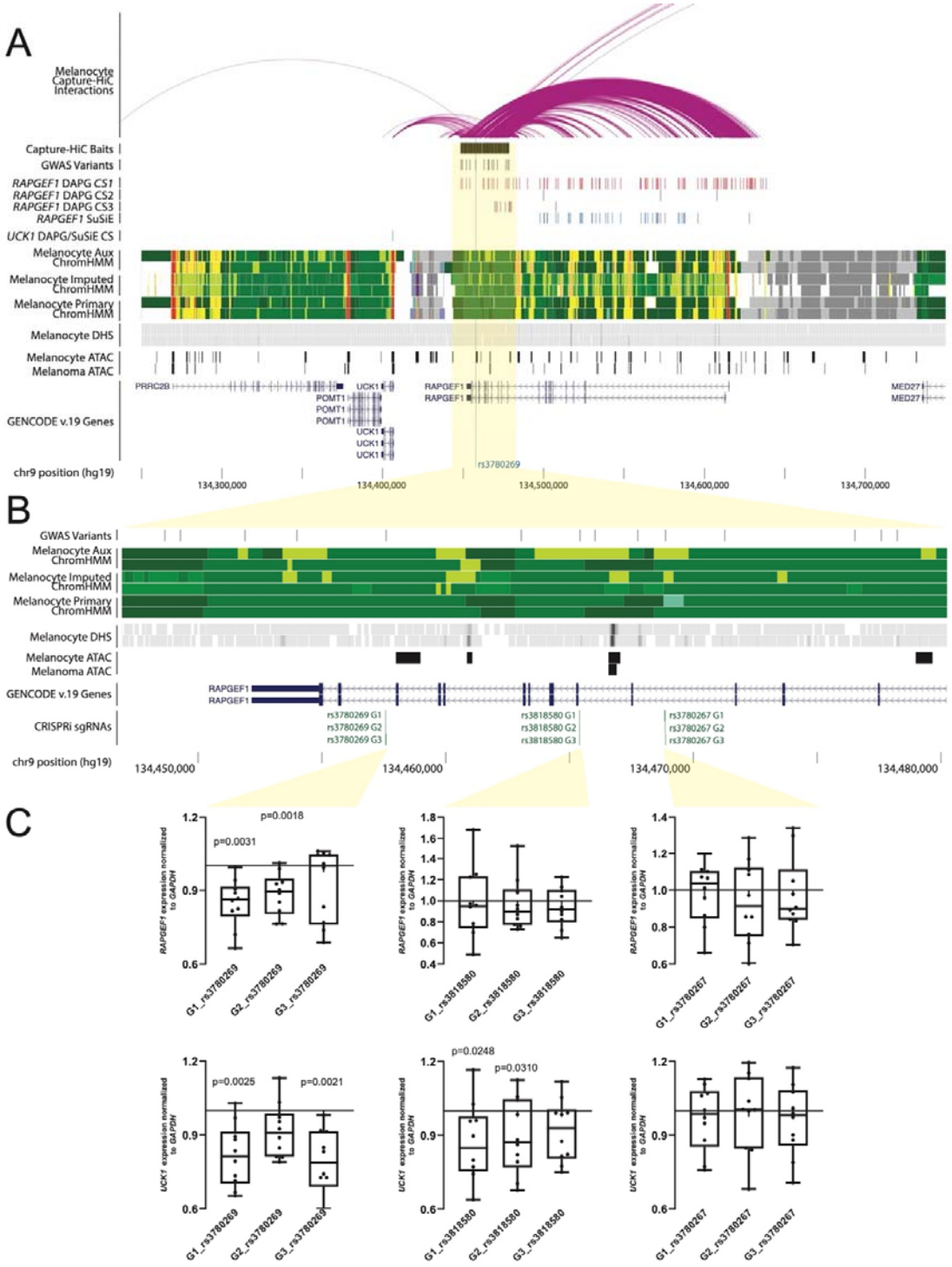

514

515 **Figure 1. Fine-mapping and epigenomic annotations of melanoma GWAS and melanocyte**
516 **eQTLs for the 9q34.13 melanoma risk locus. A.** Genetic variants fine-mapped for the
517 melanoma GWAS are annotated, along with Bayesian fine-mapped variant credible sets (CS)
518 from SuSiE and DAP-G for human primary melanocyte eQTLs for *RAPGEF1* and *UCK1*.
519 Roadmap chromatin states (ChromHMM) from primary melanocytes are shown; red and
520 orange denote annotated promoter, yellow and light green enhancer. Chromatin

accessibility from DNAse I hypersensitivity sequencing (DHS) and ATAC-sequencing (ATAC) of melanocytes and melanoma cell models is shown. Chromatin interactions between the entire region of association (Capture-HiC baits) in human melanocytes is shown; fine-mapped variants interact with the promoters of both *RAPGEF1*, *UCK1*, and *NTNG2* (not shown on figure). **B**. Zoomed in view of the fine-mapped variants. The locations of small guide RNAs used for CRISPR-inhibition (CRISPRi sgRNAs) experiments are shown. **C**. CRISPR-inhibition (CRISPRi) validation of *RAPGEF1 and UCK1* as *cis*-regulatory targets at 9q34.13. Guide RNAs were designed to target three fine-mapped variants within an ~11.3 kb interval. Each guide was individually tested for effects on *RAPGEF1 and UCK1* expression relative to the average of two non-targeting guides in immortalized melanocytes stably expressing dCas9-KRAB via a TaqMan quantitative RT-PCR assay. Whiskers show minimum and maximum values. *P*-values were calculated using a two-sample two-sided paired t-test comparing $2^{\wedge(\text{delta-Ct})}$ values from individual guides to those from the average of the two non-targeting guides with 10 biological replicates in total.

RAPGEF1 and UCK1 are cis-regulatory targets at the 9q34.13 melanoma risk locus in melanocytic cells

Transcriptome wide association studies (TWAS) using eQTL data from human primary melanocytes (n=106) [13] as well as primary melanoma tumors from TCGA (n=103) [14, 15, 80] collectively implicate two genes in the region, with melanoma risk positively associated with predicted melanocyte and melanoma expression of *RAPGEF1* ($P_{\text{melanocyte}} = 4.8 \times 10^{-5}$; $P_{\text{melanoma}} = 4.7 \times 10^{-5}$) and negatively associated with melanocyte *UCK1* ($P_{\text{melanocyte}} = 1.8 \times 10^{-5}$; **Supplementary Table 17**; *UCK1* was not included as a predictable gene from the melanoma dataset). Consistent with TWAS, which considers the collective effects of multiple sequence variants, the risk allele of rs3780269 itself is individually associated with higher *RAPGEF1* in both melanocytes and melanomas ($P = 1.4 \times 10^{-11}$ and $P = 5 \times 10^{-4}$, respectively; **Supplementary Figure 3A, Supplementary Table 18, Supplementary Table 19, Supplementary Table 20**) and negatively but not significantly associated with *UCK1* (*P* = 0.22; **Supplementary Figure 3A**, **Supplementary Table 18**).

In contrast to melanoma GWAS fine-mapping results which suggest a single signal, colocalization and fine-mapping of *RAPGEF1* and *UCK1* eQTL signals point to potentially distinct *cis*-regulatory variants for *RAPGEF1* and *UCK1*, each in partial LD with rs3780269. Melanocyte eQTL results show different lead SNPs for *RAPGEF1* (rs13295485, $P_{\text{eQTL}} = 2.8 \times 10^{-20}$, $P_{\text{GWAS}} = 4.8 \times 10^{-5}$) and *UCK1* (rs7867616, $P_{\text{eQTL}} = 2.8 \times 10^{-20}$; $P_{\text{GWAS}} = 3.3 \times 10^{-5}$; **Supplementary Tables 21, 22**), each in partial LD with rs3780269 (1000G EUR $r^2 = 0.50$, D' =

0.74 for rs13295485; $r^2 = 0.17$, D' = 0.66 for rs7867616) and each other ($r^2 = 0.12$, D' = 0.5). Analyses of GWAS and eQTL signals using multiple Bayesian approaches (SuSiE + COLOC [54] and SharePro [55]) do not provide support for colocalization of these eQTLs with the melanoma GWAS (**Supplementary Tables 23, 24; Supplementary Figure 3B, C**). Fine-mapping the *RAPGEF1* eQTL in melanocytes reveals multiple sets of CCVs collectively containing over 100 variants and spanning the entire gene and promoter (**Figure 1A**, **Supplementary Table 25**); critically several overlap the set of melanoma CCVs (**Supplementary Table 12**). The single fine-mapped *UCK1* eQTL credible set variant overlaps annotated *UCK1* promoter (rs7867616, **Figure 1A**, **Supplementary Table 26**) but not the melanoma credible set. Consistent with the eQTL data, we note a strikingly similar pattern in melanocyte methylation QTL (meQTL) data (see **Supplementary Material**), where a methylome-wide association study identified significant CpG methylation probes in both genes and individual meQTL signals mirror eQTL signals for the respective genes. These data collectively reflect a complex *cis*-regulatory structure underlying the 9q34.13 association signal.

Contributions of RAPGEF1 and UCK1 expression to the melanoma association signal

To further reinforce *RAPGEF1* and or *UCK1* as strong causal candidates regulated by a complex pattern of *cis*-regulatory signals, we performed additional conditional GWAS analyses. Conditioning on predicted melanocyte *RAPGEF1* and *UCK1* expression each partially attenuated the GWAS signal for lead SNP rs3780269 ($P_{GWAS} = 1.9 \times 10^{-8}$, *RAPGEF1* $P_{conditional} = 1.0 \times 10^{-4}$; *UCK1* $P_{conditional} = 2.1 \times 10^{-5}$; **Supplementary Table 27, 28**). When both genes were included in a joint model, both are significant (**Supplementary Table 29**) and the signal for rs3780269 is dramatically attenuated ($P_{conditional} = 0.002$; **Supplementary Table 30**). We observe similar results when instead conditioning on respective lead eQTL SNPs (*RAPGEF1* $P_{conditional} = 4.9 \times 10^{-3}$, *UCK1* $P_{conditional} = 6.33 \times 10^{-5}$; **Supplementary Table 31, 32; Supplementary Figure 1B, 1C)**, suggesting a contribution of *cis*-regulatory variants for both genes to the melanoma risk signal. We note that conditioning only on the fine-mapped *RAPGEF1* eQTL SNP with the highest PIP identified by DAP-G itself resulted in complete attenuation of the GWAS signal ($P_{conditional} = 0.29$, **Supplementary Table 33**, **Supplementary Figure 1D**), perhaps suggesting a critical role for *RAPGEF1*. Taken together, these results

point to multiple causal variants in partial LD to rs3780269 respectively influencing two plausible effector genes, *RAPGEF1* and *UCK1*, with both genes having opposing effects correlated with melanoma susceptibility: decreased *UCK1* expression and increased *RAPGEF1* expression are linked to risk.

RAPGEF1 and UCK1 both are critical for melanocyte growth and overexpression of RAPGEF1 stimulates melanocyte growth

Given the opposing effects for *RAPGEF1* and *UCK1* on melanoma risk, we assessed whether their expression impacts melanocyte growth and/or survival. We previously included *RAPGEF1*, but not *UCK1*, in a small pooled CRISPR proliferation screen in human melanocytes, noting the set of guides targeting *RAPGEF1* as the third most depleted amongst all genes screened ($P = 4.97 \times 10^{-6}$) [18] suggesting a strong positive role in melanocyte proliferation and or viability. Here, we validated this finding, silencing *RAPGEF1* using two independent shRNAs in immortalized human melanocytes and assessing cell proliferation by crystal violet staining and BrdU incorporation assays. Knockdown of *RAPGEF1* using both guides reduced melanocyte number as assessed by crystal violet assay (**Figure 2A, 2B**). Consistent with these data, BrdU flow cytometry revealed a significant decrease in DNA synthesis after targeting with both shRNAs, indicating a block in cell cycle progression upon *RAPGEF1* knockdown (**Figure 2C**). Parallel knockdown of *UCK1* similarly resulted in reduced proliferation in immortalized melanocytes, as evidenced by both assays (**Figures 2D-F**), mirroring the effects observed with *RAPGEF1* suppression. Critically, while a positive role for *RAPGEF1* in melanocyte proliferation is consistent with observation that increased melanocyte *RAPGEF1* is associated with melanoma risk, the essential role of *UCK1* in melanocyte proliferation contrasts with eQTL and TWAS findings which show that increased *UCK1* expression is protective against melanoma. While we cannot exclude a potential role for *UCK1* in melanoma susceptibility at the 9q34.13 locus via means other than influencing melanocyte proliferation, the strong concordance between the essential function of *RAPGEF1* in melanocyte proliferation and its elevated expression linked to increased melanoma risk led us to prioritize *RAPGEF1* for further investigation.

We then assessed whether increased *RAPGEF1* levels contributed to increased proliferation in immortalized melanocytes using a doxycycline induced promoter construct. Upon doxycycline treatment, cells showed significantly enhanced growth by crystal violet staining compared to untreated controls (**Figure 2G, H**), demonstrating that increased *RAPGEF1* expression stimulates melanocyte growth and could contribute to melanoma development. In summary, *RAPGEF1* expression influences melanocyte proliferation, with elevated levels driving increased cell growth that could in turn contribute to nevus and or melanoma development.

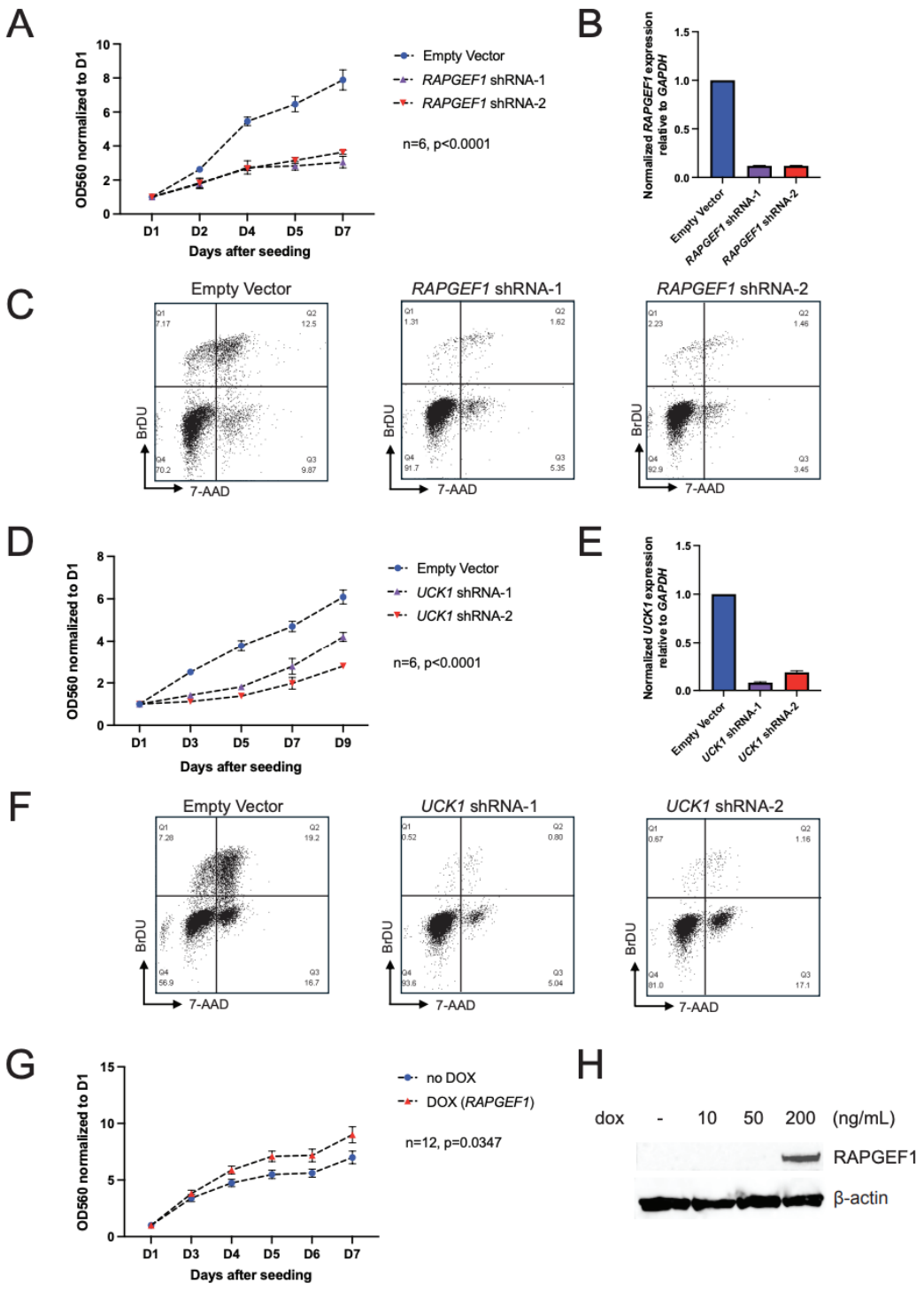

625

626 **Figure 2. RAPGEF1 and UCK1 positively regulate melanocyte proliferation. A**. Crystal
627 violet assays following *RAPGEF1* knockdown in immortalized melanocytes. Equal numbers of
628 cells either infected with two *RAPGEF1* shRNAs or vector control were seeded after infection
629 and drug selection. Cells were fixed and stained with crystal violet at multiple timepoints
630 after seeding. Crystal violet was then solubilized from stained cells and measured by OD560.
631 OD560 values were normalized to the reading at D1, and the mean of six biological

632 replicates and SEM were plotted. *P*-value was calculated from two-way ANOVA; **B**.
633 Quantitative RT-PCR for *RAPGEF1* in immortalized melanocytes following infection with
634 shRNAs targeting *RAPGEF1* relative to empty vector control. RNA was collected and assayed
635 at D5 after infection. **C**. FACS analysis of immortalized melanocytes infected with either
636 empty vector or *RAPGEF1* shRNA at D5 after infection. BrdU and 7-AAD staining were used
637 to characterize the cell cycle status of different cells. The images shown here are from a
638 representative experiment from three biological replicates. **D**. Crystal violet assays following
639 *UCK1* knockdown in immortalized melanocytes. Equal numbers of cells either infected with
640 two *UCK1* shRNAs or vector control were seeded after infection and drug selection. Cells
641 were fixed and stained with crystal violet at multiple timepoints after seeding. Crystal violet
642 was then solubilized from stained cells and measured by OD560. OD560 values were
643 normalized to the reading at D1, and the mean of six biological replicates and SEM were
644 plotted. *P*-value was calculated from two-way ANOVA. **E**. Quantitative RT-PCR for *UCK1* in
645 immortalized melanocytes following infection with shRNAs targeting *UCK1* relative to empty
646 vector control. RNA was collected and assayed at D7 after infection **F**. FACS analysis of
647 immortalized melanocytes infected with either empty vector or *UCK1* shRNA at D7 after
648 infection. BrdU and 7-AAD staining were used to characterize the cell cycle status of
649 different cells. The images shown here are from a representative experiment from three
650 biological replicates. **G**. Immortalized melanocytes infected with a dox-inducible vector
651 (pCW57.1) to express *RAPGEF1* were seeded after infection and drug selection. Dox-treated
652 cells were treated with 200ng/mL dox at seeding (D0) and cells were fixed and stained with
653 crystal violet at multiple timepoints after seeding. Crystal violet was then solubilized from
654 stained cells and measured by OD560. OD560 values were normalized to the reading of D1
655 and the mean of 12 biological replicates and SEM were plotted. *P*-value was calculated using
656 two-way ANOVA. **H**. Western blot for RAPGEF1 in dox-treated immortalized melanocytes.
657 Whole cell extract was collected 48 hours post-dox treatment at D7 after infection.

658

659 *RAPGEF1 overexpression triggers malignant transformation of human melanocytes*

660 Having established that *RAPGEF1* overexpression enhances melanocyte growth, we next
661 investigated whether *RAPGEF1* functions as a potential oncogene capable of promoting
662 malignant transformation. While RAPGEF1 has diverse roles in cancer depending on the
663 cellular context, tumor type, and stage, its function as a GEF for the small GTPase protein
664 RAP1 is central to its potential oncogenic activity. Mechanistically, RAP1 can initiate and
665 maintain MAPK/PI3K signaling, which can trigger malignant transformation of cells. To
666 further evaluate whether *RAPGEF1* can stimulate malignant transformation by affecting
667 melanocyte growth, we examined the potential effect of RAPGEF1 on anchorage-
668 independent growth of TERT-immortalized human melanocytes (p'mel cells) by soft-agar
669 colony formation assay. While p'mel cells themselves do not efficiently form large colonies
670 in soft-agar, stably expressing $BRAF^{V600E}$ in p'mel together with other oncogenes lead to
671 colony formation [81, 82]. NRAS and its constitutively active mutants have been shown to

672 promote malignant cellular transformation in multiple cells of different origins [83, 84] while
673 the direct role of RAP1 in cellular transformation has not been well-reported. Here, we
674 observed enhanced colony formation (>70 µm) in p'mel cells stably expressing both
675 $BRAF^{V600E}$ and constitutively activated NRAS, specifically $NRAS^{G12V}$ or $NRAS^{Q61R}$ ($P < 0.0001$, P
676 < 0.0001, respectively; **Figure 3A, B**) relative to those expressing $BRAF^{V600E}$ alone. Not
677 surprisingly, enhanced colony formation was also observed in p'mel cells stably expressing
678 both $BRAF^{V600E}$ and a synthetic constitutively activated $RAP1A^{G12V}$ mutant (P < 0.0001). By
679 introducing RAPGEF1 overexpression in p'mel cells, we observed that RAPGEF1 similarly
680 cooperated with *BRAF*^{V600E} to enhance colony formation ($P < 0.0001$). The $NRAS^{Q61R}$ mutant
681 induced a stronger colony formation effect than the $NRAS^{G12V}$ mutant ($P < 0.0001$),
682 consistent with *NRAS* mutations at codon 12 (such as G12V) generally exhibiting
683 intermediate oncogenic potency compared to the stronger activating mutations at codon 61
684 [85]. The number of colonies formed upon *RAPGEF1* overexpression was lower than those
685 induced by $NRAS^{Q61R}$ ($P < 0.0001$) and $RAP1A^{G12V}$ ($P = 0.0002$), but on a more similar level to
686 wild-type RAP1A ($P = 0.10$) or $NRAS^{G12V}$ ($P = 0.32$; **Figure 3A, B**). We note that we did not
687 observe such cooperation in a $BRAF^{V600E}$-expressing zebrafish model
688 (*Tg(mitfa:BRAF(V600E));p53*$^{-/-}$) [67], where overexpression of human RAPGEF1 did not
689 accelerate formation of cancer precursor zones (CPZs; $P = 0.11$) or tumors ($P = 0.21$), nor
690 was RAPGEF1 overexpression sufficient to drive tumor formation in fish that did not
691 overexpress $BRAF^{V600E}$. Overall, these data suggest that *RAPGEF1* possesses an intermediate
692 level of oncogenic potential, contributing to colony formation in melanocytes but
693 insufficient to drive tumorigenesis in the absence of a strong oncogenic mutation *in vivo*.

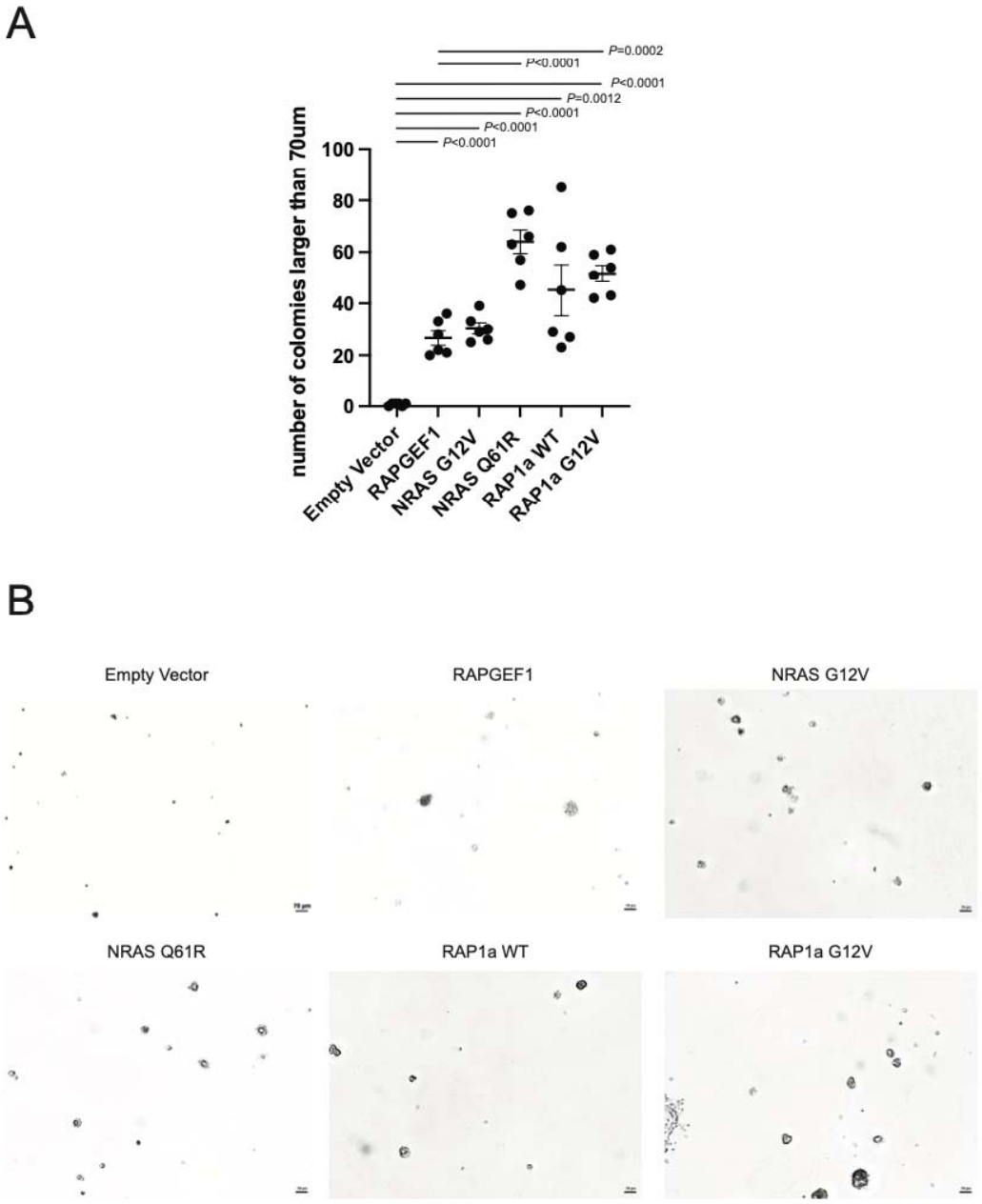

694

695 **Figure 3. Colony formation in soft agar of p'mel cells stably expressing *BRAF*^{V600E} infected**
696 **with lentivirus to express either RAPGEF1, NRAS^{G12V}, NRAS^{Q61R}, RAP1A, or RAP1A^{G12V}. A**.
697 Immortalized melanocytes (p'mel cells) expressing constitutively active *BRAF*^{V600E} were
698 infected with empty pLX304 vector or constructs expressing different proteins and seeded in
699 soft-agar plates after blasticidin selection. Images were taken between week 4-5 after
700 plating, and colonies were counted from two sets of triplicates (n = 6), with counts from
701 each individual replicate shown as a dot. Whiskers show mean with SEM. *P*-values were
702 calculated using two-tailed, unpaired Student's t-test. Significance is shown only for
703 comparisons with the empty vector control and RAPGEF1 overexpression. **B**. Representative
704 images of colonies are shown. The same magnification (4x) was applied for all the images.

705

706 *RAPGEF1 overexpression in serum-starved melanocytes potentiates activation of both RAS*
707 *and RAP1*

708 Since melanocyte growth and malignant transformation effects were noted for RAPGEF1
709 overexpression, we hypothesized that its overexpression promotes oncogenic activity via
710 activation of its known target RAP1. To test this, we overexpressed RAPGEF1 in melanocytic
711 cells using a tetracycline-inducible system, and RAP1 activation was assessed by pulldown
712 with RalGDS RBD beads, which selectively bind to the GTP-bound active form of RAP1.
713 Under standard melanocyte culture conditions, RAP1 activation remained minimal
714 regardless of RAPGEF1 overexpression, suggesting that cell growth supplement factors may
715 suppress or mask RAPGEF1 related effects (data not shown). However, when cells were
716 grown in supplement-free medium for 24 hours and then stimulated with human Epidermal
717 Growth Factor (hEGF), a weak, transient increase in RAP1 activation was detected in cells
718 not treated with doxycycline (dox), while dox-treated RAPGEF1 overexpressing cells showed
719 enhanced activation, with a marked increase in active RAP1 at 15 minutes following hEGF
720 treatment (**Figure 4A**). These results are consistent with previous studies showing that
721 RAPGEF1 acts as a GEF for RAP1 in mammalian cells.

722 RAP1 belongs to RAS small G-protein family which also contains NRAS, HRAS, KRAS and
723 many other RAS proteins. Almost all known GEFs for RAS family G-proteins contain a CDC25
724 homology domain as the catalytic domain, yet each GEF acts on only a small subset of the
725 RAS family members with a high selectivity [86]. While RAPGEF1 has been established as a
726 major GEF for RAP1, its role as a GEF of other RAS family proteins is controversial. *In vitro*
727 GEF assays using RAPGEF1 containing only CDC25 domain showed no activation of any RAS
728 proteins [86] whereas full-length RAPGEF1 displayed activation of R-RAS both *in vitro* and in
729 living COS7 cells [87]. At the same time, it was reported that RAP1 activation by RAPGEF1
730 might also contribute indirectly to RAS activation [88]. Given that the RAS signaling pathway
731 is a key regulator of melanoma development, RAS alterations are common in melanoma,
732 and that nearly every nevus harbors a mutation in BRAF or RAS, we asked whether RAPGEF1
733 overexpression affects RAS activation in melanocytes as we observed for RAP1. Compared
734 to controls, RAPGEF1 overexpression led to RAS activation even in the absence of hEGF,
735 with stronger RAS activation observed in RAPGEF1 overexpressing cells following hEGF

736 stimulation (**Figure 4B**). We also assessed downstream signaling activity following RAS
737 activation, noting increases in ERK and AKT activation correlating with levels of activated
738 RAS (**Figure 4B**). Notably, although RAPGEF1 overexpression enhanced both RAP1 and RAS
739 activation in response to hEGF, the kinetics of activation between RAS and RAP1 is clearly
740 different, with strong RAS activation from 2 to 15 minutes in comparison to noticeable
741 active RAP1 only at 15 minutes post hEGF treatment. These data raise the possibility that
742 the activation of RAS and RAP1 by RAPGEF1 may not happen concurrently, and may be
743 subjected to spatio-temporal regulation [89]. These data support a model in which
744 dysregulated RAPGEF1 expression amplifies not only RAP1, but also RAS signaling in
745 melanocytes, driving abnormal melanocyte proliferation and survival and contributing to
746 melanogenesis and tumor development.

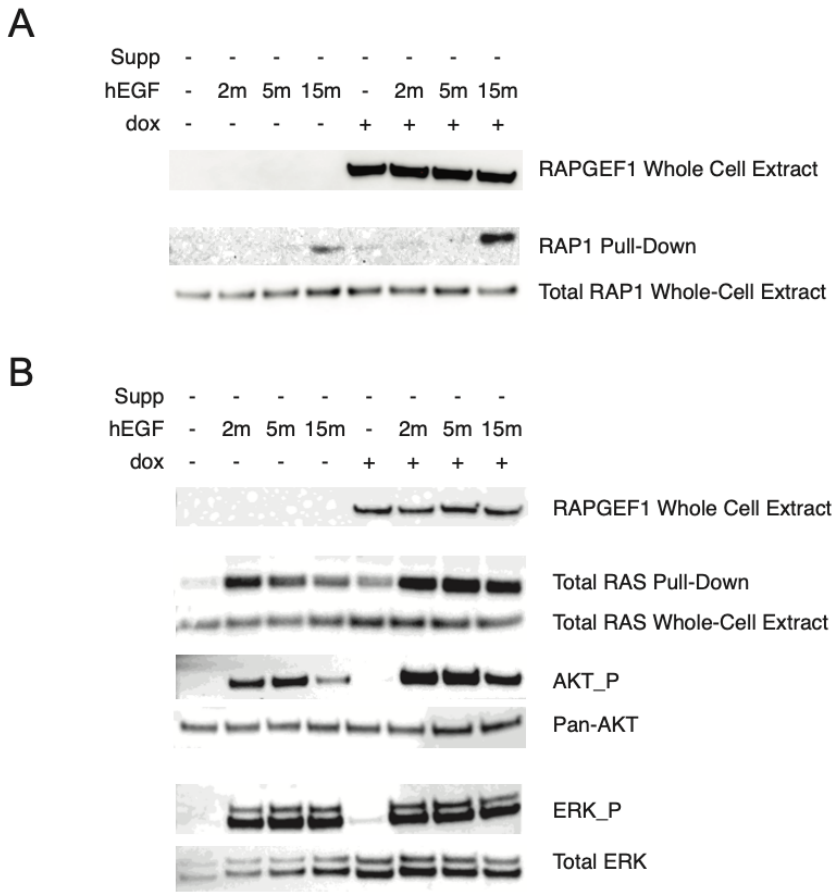

747

748

749 **Figure 4: RAPGEF1 potentiates RAP1 and RAS activation in serum starved melanocytes.**
750 C283T immortalized melanocytes with doxycycline-inducible expression of *RAPGEF1* were
751 grown in supplement-free medium for 24hrs and subsequently treated with human EGF

752 (hEGF) protein for the indicated time. **A**. Active GTP-bound RAP1 was pulled down by
753 RalGDS-RBD beads from whole-cell extract. Pull-down and whole-cell (total RAP) fractions
754 were compared by Western blotting with an antibody against RAP1. **B**. Active GTP-bound
755 RAS was pulled down by Raf-RBD beads, with the pull-down and whole-cell (total RAS)
756 fractions compared by Western blotting with an antibody against RAS. Active and total AKT
757 and ERK were compared via Western blotting. Figures are representative experiments from
758 three biological replicates.
759
760

761 *Elevated RAPGEF1 levels are associated with tumors lacking activating mutations in RAS-*
762 *MAPK signaling*

763 Hyperactivation of the RAS-MAPK signaling is a hallmark of melanoma [90, 91]. Most
764 melanomas acquire activating mutations in *BRAF* or *NRAS*, or loss-of-function mutations in
765 *NF1*, which result in constitutive RAS-MAPK pathway activation [92, 93]. In tumors lacking
766 these canonical drivers, rare mutations in other RAS-MAPK pathway members have been
767 reported to sustain RAS-MAPK signaling [14, 94-96]. In melanocytes, RAPGEF1
768 overexpression induced RAS activation in the absence of hEGF treatment. Based on this, we
769 hypothesized that *RAPGEF1* expression may act as an alternative contributor to driving RAS-
770 MAPK activation in melanoma tumors without known or strongly-activating RAS-MAPK
771 activating alterations. To test this, we analyzed RAPGEF1 expression in six publicly available
772 melanoma cohorts that included both mutation and gene expression profiling data (TCGA
773 melanoma n=366 [14], Leeds n=503 [69-71], Lund n=146 [72], Liu n=84 [73], Van Allen n=38
774 [74], Riaz n=39 [75]; **Supplementary Tables 2-8**). Since mutational data for specific strongly-
775 activating *BRAF* (codons V600 and K601) and *NRAS* (codons Q61, G12, and G13) alterations
776 across the widest range of tumors across all datasets (a subset of the Leeds cohort was only
777 assessed for these specific mutations), we initially focused on defining the RAS-MAPK wild-
778 type and mutant groups based on these specific alterations. After adjusting for clinical and
779 technical covariates (age, sex, tumor stage, and tumor purity), we consistently observed
780 significantly elevated *RAPGEF1* expression in wild-type tumors compared to the mutant
781 subgroup across five of six cohorts (TCGA $P = 3.4 \times 10^{-4}$; Leeds $P = 0.01$; Lund $P = 0.007$; Liu P
782 $= 0.004$; Van Allen $P = 0.02$), with the direction of effect in the non-significant Riaz cohort
783 consistent with the other five ($P = 0.2$) (**Supplementary Table 34; Figure 5A**). Meta-analysis
784 across these datasets showed a highly significant difference ($P_{meta} = 6.6 \times 10^{-10}$). We also
785 expanded to consider models cumulatively adding additional *BRAF* and *NRAS* driver

786 mutations (Model 2), *HRAS* and *KRAS* driver mutations (Model 3), loss-of-function *NF1*
787 mutations (Model 4), and driver alterations in other RAS-MAPK pathway members using
788 definitions from the TCGA Pan-Cancer analysis [77] (Model 5; models listed in
789 **Supplementary Table 9**). *RAPGEF1* expression remained consistently higher in the wild-type
790 subgroups in meta-analyses of each model, with the strongest association in models
791 considering driver mutations specifically in *BRAF* and *NRAS* (Model 2; $P_{model2} = 4.54 \times 10^{-10}$;
792 $P_{model3} = 1.09 \times 10^{-8}$, $P_{model4} = 2.73 \times 10^{-6}$, $P_{model5} = 1.96 \times 10^{-3}$; **Supplementary Table 34**).
793 Taken together, the consistent enrichment of *RAPGEF1* expression in tumors lacking RAS-
794 MAPK activating alterations, coupled with its ability to induce RAS, RAP, and MAPK
795 activation in melanocytes, supports a model in which *RAPGEF1* contributes to RAS-MAPK
796 pathway activation in the absence of strongly-activating canonical driver mutations.

797

798 *RAPGEF1 expression is associated with prognosis in tumors lacking RAS-MAPK activating*
799 *alterations*

800 We next evaluated whether *RAPGEF1* expression has prognostic significance in melanoma
801 tumors lacking RAS-MAPK activating alterations. Since *BRAF* (V600|K601) and *NRAS*
802 (Q61|G12|G13) hotspot alterations were profiled across most cohorts; we limited survival
803 analysis to tumors that were wild-type for these alterations. To minimize potential
804 confounding due to treatment-specific effects, we analyzed datasets comprised primarily of
805 patients not treated with immunotherapy separately from those focused on
806 immunotherapy-treatment. The Leeds, Lund, and TCGA cohorts predominantly included
807 patients who had not received immunotherapy, whereas the Liu, Van Allen, and Riaz cohorts
808 comprised immunotherapy-treated patients. *RAPGEF1* expression was dichotomized into
809 high and low groups based on a cohort-wide median cut-off for each cohort. In the analysis,
810 non-immunotherapy-treated WT tumors from TCGA (n = 92), Leeds (n = 70), and Lund (n =
811 26) cohorts, higher *RAPGEF1* expression subgroup was associated with poorer prognosis
812 compared to *RAPGEF1* low expression group (TCGA HR = 1.5, Leeds HR = 1.7, Lund HR = 2.8;
813 **Supplementary Table 35, Figure 5B**). Though these associations are below significance
814 threshold within individual cohorts, a meta-analysis of these cohorts is significant (P=0.049)
815 for *RAPGEF1* overexpression predicting shorter survival (HR = 1.6; **Supplementary Table 35;**
816 **Figure 5B**). In contrast, for cohorts of patients with WT tumors treated with immunotherapy

817 (Liu = 26, Van Allen = 16, Riaz = 14), the *RAPGEF1* high expression group was associated with
818 improved prognosis (Liu HR = 0.4, Van Allen HR = 0.2, Riaz HR = 1.03) and was significant
819 upon meta-analysis of these cohorts confirming a significant association between higher
820 *RAPGEF1* expression and longer survival (HR = 0.4, P = 0.01; **Supplementary Table 35, Figure**
821 **5B**). The opposing effects of *RAPGEF1* expression association between relatively non-treated
822 and treatment cohorts is noteworthy, however given the low sample size across most
823 cohorts, these preliminary findings should be validated in larger, independent cohorts to
824 confirm and extend these observations.

825

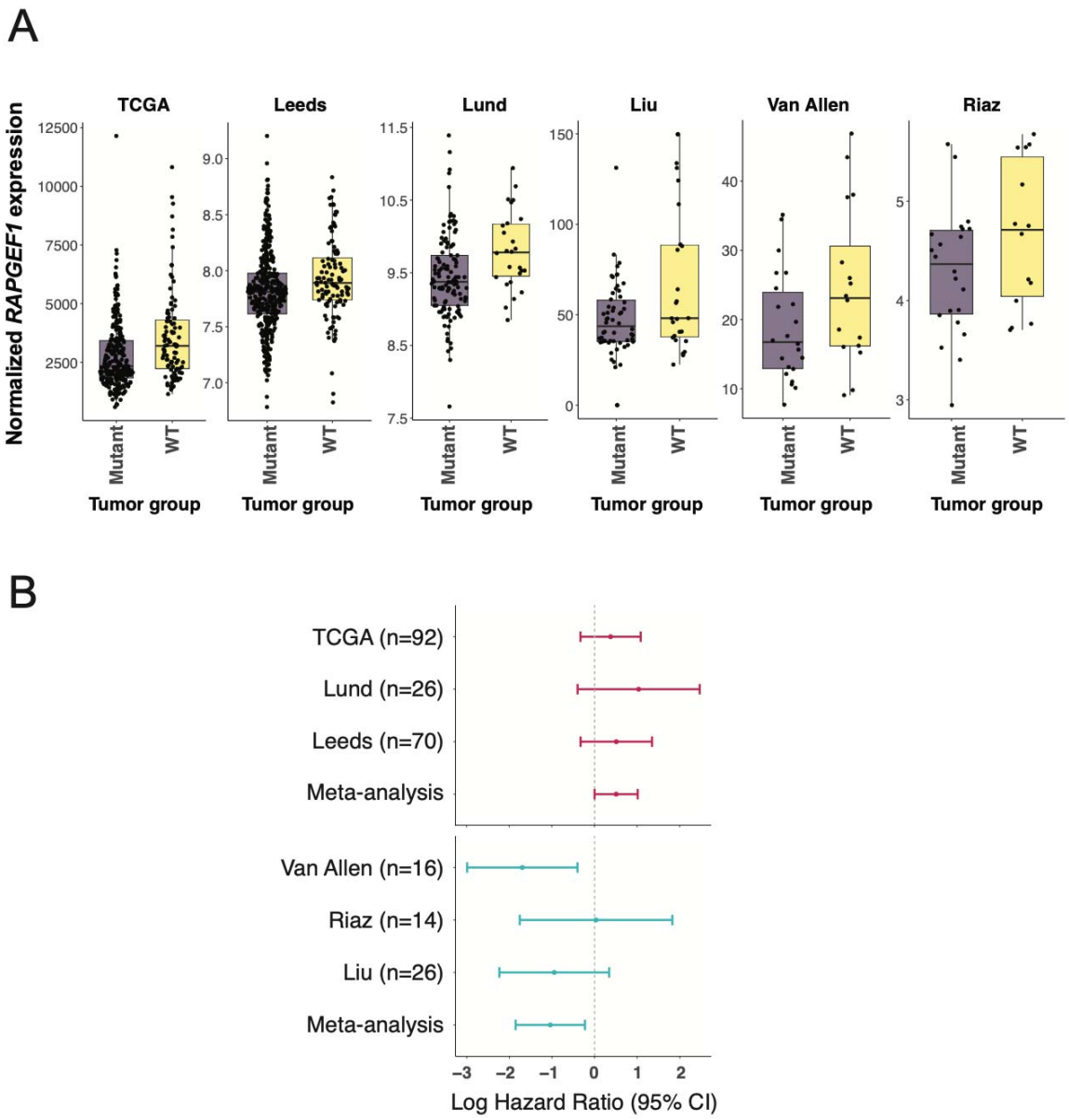

826

Figure 5: *RAPGEF1* is consistently higher in NRAS/BRAF-wild type tumors across six independent melanoma tumor cohorts. **A**. We assessed mutation and RNA expression data from six melanoma tumor cohorts: TCGA, Leeds, Lund, Liu, Riaz, and Van Allen cohorts. Within each cohort, melanoma tumors were classified into two groups: mutant and wild-type (WT) based on the presence of any *BRAF* V600 or K601 or *NRAS* Q61, G12, or G13 codon somatic mutations; tumors were designated wild-type otherwise. For each cohort, *RAPGEF1* expression distribution is visualized using boxplots. In each boxplot, the central black line represents the median expression value, upper whisker extends from the third quartile (Q3) to the largest value within 1.5x inter-quartile range (IQR) above Q3, while the lower whisker spans from the first quartile (Q1) to the smallest value within 1.5×IQR below Q1. The interquartile range (IQR) is defined as the difference between Q3 and Q1. Because expression data were normalized using a cohort-specific normalization method, *RAPGEF1* expression values are not directly comparable between cohorts. **B**. Meta-analysis across melanoma cohorts assessing *RAPGEF1* as a marker of survival in tumors wild type for *BRAF* codon V600 and K601 and *NRAS* codon Q61, G12, and G13 somatic mutations. To minimize potential confounding due to treatment-specific effects, we analyzed datasets comprised primarily of patients not treated with immunotherapy (TCGA, Lund, and Leeds cohorts) separately from those focused on immunotherapy-treatment (Van Allen, Riaz, and Liu cohorts). The variable n denotes the number of samples analyzed in the WT group for each cohort. Within each cohort, *RAPGEF1* expression was dichotomized into high and low groups based on the median value. The low *RAPGEF1* expression group is the reference group in Cox models and is depicted by the grey line on the plot. Each point represents the estimated log HR for a given cohort; horizontal lines denote the 95% confidence interval around the point estimate. The meta-analysis label on the plot denotes the log HR estimate from the meta-analysis.

Discussion

GWAS of melanoma and melanoma risk-associated phenotypes have successfully identified numerous loci associated with risk, but the causal sequence variants and genes underlying most have yet to be established. Here, we characterize a GWAS locus at 9q34.13 associated with melanoma risk as well as nevus count [1] and identify a likely role for germline variation regulating RAS and RAP signaling via modulation of expression of the guanine nucleotide exchange factor *RAPGEF1*. Given that both nevi and melanomas originate from melanocytes, we focused on quantitative trait locus (QTL) data from melanocytic cells, demonstrating an association between higher *RAPGEF1* expression and the risk allele via both colocalization and TWAS/MWAS approaches. We show that RAPGEF1 promotes both RAP1 and RAS activation in melanocytes and contributes to colony formation in immortalized melanocytes. Notably, we also observe consistently higher *RAPGEF1* levels in

866 melanomas lacking canonical, strongly-activating RAS-MAPK pathway mutations, suggesting
867 that *RAPGEF1* could potentially contribute to pathway activation in these wild-type tumors.

868 Analyses of this locus using multiple melanocytic genomic datasets (eQTL, meQTL) revealed
869 a complex pattern of LD between the melanoma GWAS signal and two partially-correlated
870 melanocyte eQTLs in the region for *RAPGEF1* and *UCK1*, complicating efforts to firmly
871 identify the causal sequence variant or variants underlying melanoma risk at this locus.
872 While conditional analysis of this GWAS locus indicates the presence of only a single signal,
873 fine-mapping of the GWAS and respective melanocyte eQTLs reveal mostly distinct sets of
874 potential causal variants for each, all in LD with each other, possibly indicating the presence
875 of functional variants in each credible set contributing to risk, or alternatively that the GWAS
876 signal may simply be an efficient tag for haplotypes containing causal *UCK1* and *RAPGEF1*
877 *cis*-regulatory variants. We demonstrated that the region harboring the GWAS signal itself
878 physically interacts with the promoters of and is a functional regulatory sequence for both
879 genes. Conditioning on predicted melanocyte expression of both *RAPGEF1* and *UCK1*
880 together does not fully attenuate the GWAS signal, suggesting a potential functional role for
881 the GWAS signal itself. Still, past MPRA work assessing fine-mapped melanoma GWAS
882 variants in both melanocytes and melanoma failed to identify variants with allele-specific
883 *cis*-regulatory activity, perhaps indicating the lack of causal variants amongst the GWAS
884 credible set or alternatively that there may be undiscovered variation strongly associated
885 with the signal, or both. Further work will be required to identify the causal *cis*-regulatory
886 variants in this region.

887 Similarly, the complex LD between GWAS and eQTL signals in this region complicate efforts
888 to firmly establish a single gene as the only likely causal gene underlying melanoma risk at
889 this locus. eQTL and meQTL analyses establish both *RAPGEF1* and *UCK1* as *cis*-regulatory
890 targets and strong candidate melanoma risk genes where higher *RAPGEF1* expression and
891 lower *UCK1* are associated with risk. Conditional analysis of the GWAS based either on
892 predicted *RAPGEF1* and *UCK1* expression, or alternatively using lead eQTL SNPs for both
893 genes showed that *RAPGEF1* expression potentially contributes more to the melanoma risk
894 signal than *UCK1*, but these data need to be interpreted cautiously given potential
895 differences in the populations from the GWAS and the relatively small sample of
896 melanocytes and melanomas used in QTL analyses.

897 We performed gene knockdown experiments in melanocytes to assess potential phenotypes
898 mediated by both genes. Knockdown of either gene resulted in dramatically decreased
899 melanocyte proliferation. Given the opposing directions of effect for melanocyte eQTLs
900 relative to melanoma risk, we chose to focus on *RAPGEF1* in melanocytes where higher
901 expression associated with risk and an observed positive effect on melanocyte growth is
902 consistent with a role promoting tumor formation or growth. Nonetheless, we cannot fully
903 exclude a role for *UCK1*, a member of the pyrimidine salvage pathway that is crucial for DNA
904 replication and repair mechanisms. We observed that RAPGEF1 overexpression in an
905 immortalized melanocyte model that expresses oncogenic BRAF (V600E) results in efficient
906 formation of large (>70um) colonies, where $BRAF^{V600E}$ expression itself is not sufficient.
907 These data are consistent with that observed for other genes with oncogenic potential in
908 melanocytes in this model [81, 82]. While colony formation in melanocytes expressing
909 constitutively active mutants of NRAS (Q61R) and RAP1A (G12V) was considerably higher
910 than that for RAPGEF1, colony formation was similar between RAPGEF1 overexpressing
911 melanocytes and those expressing the less common and potent G12V mutant of NRAS, as
912 well as overexpression of wild-type RAP1A, highlighting the oncogenic activity of RAPGEF1.

913 *RAPGEF1* is a guanine nucleotide exchange factor that facilitates the exchange of GDP for
914 GTP, thereby activating small GTPases, through interactions mediated by SH3 domains of its
915 partner proteins. Almost all known GEFs for RAS family G-proteins contain a CDC25
916 homology domain as the catalytic domain, yet each GEF acts on only a small subset of the
917 RAS family members with a high selectivity [86]. While SOS proteins are widely-
918 expressed GEFs activating RAS proteins, RAPGEF1 has been established as a major GEF for
919 RAP1 [97, 98]. Given the similarity in RAPGEF1 colony formation results as compared to
920 $NRAS^{G12V}$, and that RAPGEF1 has previously been implicated in activation of R-RAS [87] as
921 well as indirect activation of RAS [88], we assessed the effect of RAPGEF1 expression on
922 both RAP1 and RAS activation in serum starved melanocytes. Strikingly, RAPGEF1
923 overexpression contributed to both RAP1 and RAS activation upon hEGF treatment, as well
924 as leading to constitutive activation of RAS itself in the absence of hEGF suggesting RAPGEF1
925 contributes to RAS activation. Temporally, we observe that RAS activation in response to
926 hEGF appears to precede activation of RAP1, with a noticeable increase in active RAS at 2
927 minutes compared to that for RAP1 at 15 minutes.

928 While a role for direct activation of RAS by RAPGEF1 has not been established, some GEFs
929 can indeed act on both RAS and RAP1 proteins. GRP3, a GEF abundantly expressed in brain,
930 increased GTP/GDP-bound ratios of both HRAS and RAP1A in 293T cells [99]. CalDAG-GEFIII,
931 one of the four CalDAG-GEFs, promoted nuclear exchange of HRAS, R-RAS and RAP1, and
932 shows the widest substrate specificity among the known GEFs [100]. RasGRP2, an
933 alternatively spiced form of CalDAG-GEF1, selectively catalyzes nucleotide exchange on N-
934 and K-RAS, but not H-RAS. RasGRP2 also activates RAP1, albeit less potently than CalDAG-
935 GEF1, which preferentially activates RAP1 [101]. The selectivity of a substrate by a GEF is
936 largely determined by the amino acid residues at the interface between the GEF and the
937 GTPase, yet this interaction can be highly context-dependent and subjected to spatio-
938 temporal regulation [89, 102]. During *Drosophila* eye and wing development,
939 overexpression of membrane-tagged full-length *Drosophila* RAPGEF1 phenotypically mimics
940 overactivation of the RAS1–MAPK pathway, suggesting that *Drosophila* RAPGEF1 is involved
941 in RAS activation *in vivo*. These effects can be suppressed by both reduction in the gene
942 dose of RAS1–MAPK pathway components or RAP1, as well as overexpression of a
943 membrane-tagged version of *Drosophila* RAPGEF1 lacking the CDC25 catalytic domain.
944 These findings indicated that membrane localization of dysregulated RAPGEF1 can trigger
945 activation of RAP1 and RAS resulting in the activation of MAPK [102]. We did perform mass
946 spectrometry analysis of proteins pulled-down by RAPGEF1 antibody in RAPGEF1
947 overexpressing immortalized melanocytes grown either in regular melanocyte medium or
948 under serum-starved and hEGF-treated conditions, but did not identify any small GTPases
949 (including RAP1; data not shown). While the traditional affinity-purification Mass
950 spectroscopy (AP-MS) methods often require stable protein interactions in cell extracts,
951 small GTPases undergo dynamic conformational changes as they cycle between active and
952 inactive states and the transient nature of their interactions with GEFs making it difficult to
953 be captured. A typical example is SOS1, a major GEF of RAS protein, is historically
954 challenging to be captured with AP-MS [103, 104]. Interestingly, using live-cell proximity-
955 dependent biotin labelling of proteins (BioID) followed by Mass Spec analysis, Kovalski and
956 colleagues captured an interaction between HRAS and RAPGEF1 in bladder cancer cells,
957 supporting the notion that RAPGEF1 may indeed function as a GEF of HRAS [104]. Further
958 work will be required to assess whether RAPGEF1 directly acts on RAS in melanocytes,

959 however our data clearly demonstrate a role for activation of RAS by RAPGEF1 in
960 melanocytes whether directly or indirectly.

961 Most melanoma tumors harbor somatic RAS-MAPK pathway activating alterations, including
962 oncogenic mutations in RAS genes, BRAF, or loss of NF1, and likely do not need to rely on
963 more subtle germline influence on pathway-activating genes. Still, a minority of melanomas
964 lack strongly-activating RAS and BRAF mutations or alterations in other directly-involved
965 pathway members, suggesting other mechanisms likely contribute to pathway activation in
966 a subset of tumors. Given our observation that RAPGEF1 activates RAS in melanocytic cells,
967 we evaluated whether *RAPGEF1* expression differs between tumors with RAS-MAPK
968 activating mutations and those that are wild-type. Across six melanoma cohorts, we
969 consistently observed elevated *RAPGEF1* expression in wild-type tumors. These data are
970 consistent with a potential role for RAPGEF1 contributing to RAS-MAPK pathway activation
971 in these tumors, whether via an effect on RAS, RAP, or both. We also assessed whether
972 *RAPGEF1* expression in wild-type tumors could serve as a prognostic marker. Across
973 melanoma cohorts where most patients had not received any form of immunotherapy
974 treatment, *RAPGEF1* overexpression predicted poor prognosis. Conversely, in cohorts where
975 all patients were treated with immunotherapy, elevated *RAPGEF1* expression predicted
976 improved survival. Interestingly, rare somatic mutations in *RAPGEF1* have been observed in
977 non-Hodgkin's lymphomas that disrupt RAPGEF1 autoinhibition and lead to constitutive
978 RAP1 activation, suggesting a plausible role for RAPGEF1 in promoting cancer progression
979 [105]. Nonetheless, given the relative rarity of RAS-MAPK wild-type tumors and the
980 relatively small sample sizes in these patient cohorts, this association need to be treated
981 cautiously and more rigorously validated.

982 Rare germline variation in RAS pathway genes is known to impact nevus development,
983 specifically strong activating germline mutations that cause developmental syndromes
984 termed "RASopathies" [106]; patients with select RASopathies have higher number of
985 melanocytic nevi [107-109]. Together with recent data potentially implicating other RAS-
986 pathway members in melanoma/nevus risk loci, our data contribute to emerging evidence
987 that common germline variation in genes regulating RAS pathway activity may also play a
988 prominent role in melanoma risk and nevus development. We previously used a GWAS
989 region-focused capture-HiC assay to nominate potential target genes from other melanoma

990 GWAS loci [22], with *CBL* and *SHC1* nominated at separate loci. *CBL* encodes a negative
991 regulator of receptor tyrosine kinases (and in turn, RAS signaling). We previously validated
992 that the risk allele at the respective locus was associated with decreased *CBL* expression and
993 demonstrated regulation of *CBL* by the region of the risk signal [22]. *SHC1*, which was
994 nominated by the observation of active enhancer-promoter interactions from regions
995 surrounding fine-mapped risk variants, encodes an adaptor protein that transduces signals
996 from activated receptors to RAS by recruiting GRB2-SOS complexes, thereby promoting RAS
997 activation and downstream RAS-MAPK signaling [110, 111]. In addition, the gene encoding
998 another RAP GEF (*RAPGEF5*) is located at a melanoma risk locus identified by Landi and
999 colleagues (rs12539524) [1], raising the possibility that other such GEFs could play a similar
1000 role. Lastly, a new GWAS of nevus count that nominated *NRAS* itself as a potential causal
1001 gene at a novel locus marked by rs7537232 [112]. While nearly every nevus acquires an
1002 oncogenic mutation in either *BRAF* or *NRAS*, our data suggest that germline variation
1003 regulating RAS activity may confer a growth or survival advantage prior to acquisition of a
1004 strongly activating somatic mutation.

1005 We note several limitations of our study. Firstly, we have not positively identified the causal
1006 variant or variants underlying risk at this locus. Efforts to do so statistically are hampered by
1007 partial LD between QTL and melanoma risk signals, as well as a very large number of
1008 potential causal variants for melanocyte *RAPGEF1* expression. Nonetheless, the evidence
1009 implicating *RAPGEF1*, and perhaps *UCK1*, at this locus is strong. As noted above, we cannot
1010 rule out a role for *UCK1* in melanoma risk, further work will be required to assess potential
1011 phenotypes associated with variation in *UCK1* levels in melanocytes. Critically, while we
1012 have established that RAPGEF1 dysregulation leads to RAS activation, we have not
1013 demonstrated that RAPGEF1 acts as a direct GEF for RAS. We show a strong association of
1014 *RAPGEF1* levels with mutation status in melanoma tumors, however further work is
1015 required to establish whether and or to what degree RAPGEF1 actively contributes to RAS-
1016 MAPK pathway activation in tumors. Finally, the melanoma survival datasets are each
1017 relatively small, with even smaller numbers of RAS-MAPK pathway wild-type tumors; further
1018 assessment of associations of *RAPGEF1* with survival in patients with wild-type tumors is
1019 needed.

1020

Acknowledgements

This research was supported in part by the Intramural Research Program of the National Institutes of Health (NIH). The contributions of the NIH author(s) are considered Works of the United States Government. The findings and conclusions presented in this paper are those of the author(s) and do not necessarily reflect the views of the NIH or the U.S. Department of Health and Human Services. This work utilized the Biowulf cluster computing system at the NIH. The results appearing here are in part based on data generated by the TCGA Research Network. We would like to thank members at the National Cancer Institute Cancer Genomics Research Laboratory (CGR) for their help with sequencing efforts. We also thank all the cohorts, funders, and investigators who contributed to the melanoma GWAS, as originally acknowledged by Landi and colleagues. We would like to thank the research participants and employees of 23andMe. Mark Iles is supported in part by the National Institute for Health and Care Research (NIHR) Leeds Biomedical Research Centre. The views expressed are those of the author(s) and not necessarily those of the NHS, the NIHR or the Department of Health and Social Care. The Leeds Melanoma Cohort was funded by CRUK grants C588/A19167, C8216/A6129, C588/A10721 and NIH grant CA83115. JN is supported by Horizon Europe grant 101136622.

Declaration of Interests

The authors declare no competing interests.

Web Resources

- NIH Biowulf Cluster, http://hpc.nih.gov
- PLINK: https://www.cog-genomics.org/plink/
- GCTA-COJO : https://yanglab.westlake.edu.cn/software/gcta/
- RSparsePro: https://github.com/zhwm/RSparsePro_LD
- SuSiE: https: https://stephenslab.github.io/susieR/reference/susie_rss.html
- DAP-G: https://github.com/xqwen/dap

1049 • AREsite2: http://nibiru.tbi.univie.ac.at/AREsite2/welcome
1050 • Ensembl variant Effect Predictor:
1051 https://useast.ensembl.org/info/docs/tools/vep/index.html
1052 • TWAS FUSION: http://gusevlab.org/projects/fusion/
1053 • COLOC: https://github.com/chr1swallace/coloc
1054 • SharePro: https://github.com/zhwm/SharePro_coloc
1055 • ENCODE: https://www.encodeproject.org/encyclopedia/
1056 • CHiCAGO: https://www.functionalgenecontrol.group/chicago
1057 • HiCUP: https://www.bioinformatics.babraham.ac.uk/projects/hicup/
1058 • LDlink: https://ldlink.nih.gov/?tab=home
1059 • UCSC browser: https://genome.ucsc.edu
1060 • WashU Epigenome Browser: http://epigenomegateway.wustl.edu
1061 • Bedtools: https://bedtools.readthedocs.io/en/latest/
1062 • Bedtoolsr: http://phanstiel-lab.med.unc.edu/bedtoolsr.html
1063 • ROADMAP epigenomic project:
1064 https://egg2.wustl.edu/roadmap/web_portal/chr_state_learning.html
1065 • TCGA melanoma cohort:
1066 https://www.cbioportal.org/study/summary?id=skcm_tcga_pan_can_atlas_2018
1067 • Van Allen cohort data:
1068 https://www.cbioportal.org/study/summary?id=skcm_dfci_2015)
1069 • Liu Cohort data: https://www.cbioportal.org/study/summary?id=mel_dfci_2019)
1070 • Riaz cohort data: https://github.com/riazn/bms038_analysis/tree/master/data
1071

1072 **Data and Code Availability**

1073 Small RNA-seq data generated from 106 melanocyte cultures is currently being deposited on
1074 ArrayExpress. Melanocyte ATAC-seq and capture-HiC data are publicly available
1075 (ArrayExpress accession: E-MTAB-15079, E-MTAB-15048). Melanocyte genotyping, RNA-
1076 sequencing, and methylation data are previously published [13, 16] and accessible through
1077 NCBI database of Genotypes and Phenotypes (dbGaP) under accession dbGaP:
1078 phs001500.v2.p1.

1079 MPRA are previously published [23]; raw sequencing can be accessed through NCBI Gene
1080 Expression Omnibus (GEO; https://www.ncbi.nlm.nih.gov/geo/) under the accession
1081 GEO: GSE210356.

1082 Summary data for 2020 melanoma GWAS were obtained from dbGaP (dbGaP:
1083 phs001868.v1.p1), with the exclusion of self-reported data from 23andMe, Inc. and UK
1084 Biobank. The full GWAS summary statistics for the 23andMe discovery dataset will be made
1085 available through 23andMe to qualified researchers under an agreement with 23andMe
1086 that protects the privacy of the 23andMe participants. Please
1087 visit https://research.23andme.com/collaborate/#dataset-access/ for more information and
1088 to apply to access the data. Summary data from the remaining self-reported cases are
1089 available from the corresponding authors of that manuscript (Matthew
1090 Law, matthew.law@qimrberghofer.edu.au; Mark Iles, m.m.iles@leeds.ac.uk; and Maria
1091 Teresa Landi, landim@mail.nih.gov).

1092 Melanoma tumor data for TCGA melanoma cohort was accessed using cBioportal database
1093 https://www.cbioportal.org/study/summary?id=skcm_tcga_pan_can_atlas_2018.

1094 Leeds Melanoma cohort gene expression and mutation profiling dataset is available on
1095 European Genome-phenome Archive (study ID: EGAS00001002922, dataset ID:
1096 EGAD00010001561, dataset ID: EGAD00001008360). Lund Melanoma gene expression
1097 dataset is available on NCBI Gene Expression Omnibus (GSE65904); mutation profiling data
1098 was available from Cirenajwis *et al.*, Supplementary Table 3 [72]. Liu and Van Allen cohort
1099 dataset was accessed using cBioportal (Liu cohort:
1100 https://www.cbioportal.org/study/summary?id=mel_dfci_2019) (Van Allen cohort:
1101 https://www.cbioportal.org/study/summary?id=skcm_dfci_2015) Riaz cohort mutation and
1102 expression dataset was accessed using
1103 https://github.com/riazn/bms038_analysis/tree/master/data

1104

1105 **Author Contributions**

1106 R.T., M.X, H.S., J.Yon, S.A.-S., M.L., T.R., H.S., G.D., L.J., T.M, T.Z., R.C., E.L., K.F., J.Yin, R.H.,
1107 T.Z., G.J., D.T.B., J.N.-B., J.N., M.M.I., M.T.L., M.H.L., T.A., J.C., J.S., and K.M.B. contributed to

the research activities described in this manuscript. K.M.B. led and supervised the research described. M.M. provided additional supervision and mentorship. R.T., M.X., and K.M.B. wrote the manuscript.

References

1. Landi, M.T., D.T. Bishop, S. MacGregor, M.J. Machiela, A.J. Stratigos, P. Ghiorzo, M. Brossard, D. Calista, J. Choi, M.C. Fargnoli, T. Zhang, M. Rodolfo, A.J. Trower, C. Menin, J. Martinez, A. Hadjisavvas, L. Song, I. Stefanaki, R. Scolyer, R. Yang, A.M. Goldstein, M. Potrony, K.P. Kypreou, L. Pastorino, P. Queirolo, C. Pellegrini, L. Cattaneo, M. Zawistowski, P. Gimenez-Xavier, A. Rodriguez, L. Elefanti, S. Manoukian, L. Rivoltini, B.H. Smith, M.A. Loizidou, L. Del Regno, D. Massi, M. Mandala, K. Khosrotehrani, L.A. Akslen, C.I. Amos, P.A. Andresen, M.F. Avril, E. Azizi, H.P. Soyer, V. Bataille, B. Dalmasso, L.M. Bowdler, K.P. Burdon, W.V. Chen, V. Codd, J.E. Craig, T. Debniak, M. Falchi, S. Fang, E. Friedman, S. Simi, P. Galan, Z. Garcia-Casado, E.M. Gillanders, S. Gordon, A. Green, N.A. Gruis, J. Hansson, M. Harland, J. Harris, P. Helsing, A. Henders, M. Hocevar, V. Hoiom, D. Hunter, C. Ingvar, R. Kumar, J. Lang, G.M. Lathrop, J.E. Lee, X. Li, J. Lubinski, R.M. Mackie, M. Malt, J. Malvehy, K. McAloney, H. Mohamdi, A. Molven, E.K. Moses, R.E. Neale, S. Novakovic, D.R. Nyholt, H. Olsson, N. Orr, L.G. Fritsche, J.A. Puig-Butille, A.A. Qureshi, G.L. Radford-Smith, J. Randerson-Moor, C. Requena, C. Rowe, N.J. Samani, M. Sanna, D. Schadendorf, H.J. Schulze, L.A. Simms, M. Smithers, F. Song, A.J. Swerdlow, N. van der Stoep, N.A. Kukutsch, A. Visconti, L. Wallace, S.V. Ward, L. Wheeler, R.A. Sturm, A. Hutchinson, K. Jones, M. Malasky, A. Vogt, W. Zhou, K.A. Pooley, D.E. Elder, J. Han, B. Hicks, N.K. Hayward, P.A. Kanetsky, C. Brummett, G.W. Montgomery, C.M. Olsen, C. Hayward, A.M. Dunning, N.G. Martin, E. Evangelou, G.J. Mann, G. Long, P.D.P. Pharoah, D.F. Easton, J.H. Barrett, A.E. Cust, G. Abecasis, D.L. Duffy, D.C. Whiteman, H. Gogas, A. De Nicolo, M.A. Tucker, J.A. Newton-Bishop, M.E.L.C. Geno, M. Q, Q. Investigators, A.M.S. Group, andMe, S.D.H.S. Group, I.B.D. Investigators, I. Essen-Heidelberg, A. Investigators, C. MelaNostrum, K. Peris, S.J. Chanock, F. Demenais, K.M. Brown, S. Puig, E. Nagore, J. Shi, M.M. Iles and M.H. Law, *Genome-wide association meta-analyses combining multiple risk phenotypes provide insights into the genetic architecture of cutaneous melanoma susceptibility.* Nat Genet, 2020. **52**(5): p. 494-504.
2. Cano-Gamez, E. and G. Trynka, *From GWAS to Function: Using Functional Genomics to Identify the Mechanisms Underlying Complex Diseases.* Front Genet, 2020. **11**: p. 424.
3. Gallagher, M.D. and A.S. Chen-Plotkin, *The Post-GWAS Era: From Association to Function.* Am J Hum Genet, 2018. **102**(5): p. 717-730.
4. Flynn, E.D. and T. Lappalainen, *Functional Characterization of Genetic Variant Effects on Expression.* Annu Rev Biomed Data Sci, 2022. **5**: p. 119-139.
5. Consortium, G.T., *The GTEx Consortium atlas of genetic regulatory effects across human tissues.* Science, 2020. **369**(6509): p. 1318-1330.
6. Duffy, D.L., Z.Z. Zhao, R.A. Sturm, N.K. Hayward, N.G. Martin, and G.W. Montgomery, *Multiple pigmentation gene polymorphisms account for a substantial proportion of risk of cutaneous malignant melanoma.* J Invest Dermatol, 2010. **130**(2): p. 520-8.
7. Bataille, V., B.S. Kato, M. Falchi, J. Gardner, M. Kimura, M. Lens, U. Perks, A.M. Valdes, D.C. Bennett, A. Aviv, and T.D. Spector, *Nevus size and number are associated with telomere length and represent potential markers of a decreased senescence in vivo.* Cancer Epidemiol Biomarkers Prev, 2007. **16**(7): p. 1499-502.
8. Codd, V., C.P. Nelson, E. Albrecht, M. Mangino, J. Deelen, J.L. Buxton, J.J. Hottenga, K. Fischer, T. Esko, I. Surakka, L. Broer, D.R. Nyholt, I. Mateo Leach, P. Salo, S. Hagg, M.K. Matthews, J. Palmen, G.D. Norata, P.F. O'Reilly, D. Saleheen, N. Amin, A.J. Balmforth, M. Beekman, R.A. de Boer, S. Bohringer, P.S. Braund, P.R. Burton, A.J. de Craen, M. Denniff, Y. Dong, K. Douroudis, E. Dubinina, J.G. Eriksson, K. Garlaschelli, D. Guo, A.L. Hartikainen, A.K. Henders, J.J. Houwing-Duistermaat, L. Kananen, L.C. Karssen, J. Kettunen, N. Klopp, V. Lagou, E.M. van Leeuwen, P.A.

Madden, R. Magi, P.K. Magnusson, S. Mannisto, M.I. McCarthy, S.E. Medland, E. Mihailov, G.W. Montgomery, B.A. Oostra, A. Palotie, A. Peters, H. Pollard, A. Pouta, I. Prokopenko, S. Ripatti, V. Salomaa, H.E. Suchiman, A.M. Valdes, N. Verweij, A. Vinuela, X. Wang, H.E. Wichmann, E. Widen, G. Willemsen, M.J. Wright, K. Xia, X. Xiao, D.J. van Veldhuisen, A.L. Catapano, M.D. Tobin, A.S. Hall, A.I. Blakemore, W.H. van Gilst, H. Zhu, C.A. consortium, J. Erdmann, M.P. Reilly, S. Kathiresan, H. Schunkert, P.J. Talmud, N.L. Pedersen, M. Perola, W. Ouwehand, J. Kaprio, N.G. Martin, C.M. van Duijn, I. Hovatta, C. Gieger, A. Metspalu, D.I. Boomsma, M.R. Jarvelin, P.E. Slagboom, J.R. Thompson, T.D. Spector, P. van der Harst, and N.J. Samani, *Identification of seven loci affecting mean telomere length and their association with disease.* Nat Genet, 2013. **45**(4): p. 422-7, 427e1-2.

9. Han, J., A.A. Qureshi, J. Prescott, Q. Guo, L. Ye, D.J. Hunter, and I. De Vivo, *A prospective study of telomere length and the risk of skin cancer.* J Invest Dermatol, 2009. **129**(2): p. 415-21.

10. Duffy, D.L., G. Zhu, X. Li, M. Sanna, M.M. Iles, L.C. Jacobs, D.M. Evans, S. Yazar, J. Beesley, M.H. Law, P. Kraft, A. Visconti, J.C. Taylor, F. Liu, M.J. Wright, A.K. Henders, L. Bowdler, D. Glass, M.A. Ikram, A.G. Uitterlinden, P.A. Madden, A.C. Heath, E.C. Nelson, A.C. Green, S. Chanock, J.H. Barrett, M.A. Brown, N.K. Hayward, S. MacGregor, R.A. Sturm, A.W. Hewitt, G.C. Melanoma, M. Kayser, D.J. Hunter, J.A. Newton Bishop, T.D. Spector, G.W. Montgomery, D.A. Mackey, G.D. Smith, T.E. Nijsten, D.T. Bishop, V. Bataille, M. Falchi, J. Han, and N.G. Martin, *Novel pleiotropic risk loci for melanoma and nevus density implicate multiple biological pathways.* Nat Commun, 2018. **9**(1): p. 4774.

11. Chang, Y.M., J.A. Newton-Bishop, D.T. Bishop, B.K. Armstrong, V. Bataille, W. Bergman, M. Berwick, P.M. Bracci, J.M. Elwood, M.S. Ernstoff, A.C. Green, N.A. Gruis, E.A. Holly, C. Ingvar, P.A. Kanetsky, M.R. Karagas, L. Le Marchand, R.M. Mackie, H. Olsson, A. Osterlind, T.R. Rebbeck, K. Reich, P. Sasieni, V. Siskind, A.J. Swerdlow, L. Titus-Ernstoff, M.S. Zens, A. Ziegler, and J.H. Barrett, *A pooled analysis of melanocytic nevus phenotype and the risk of cutaneous melanoma at different latitudes.* Int J Cancer, 2009. **124**(2): p. 420-8.

12. Olsen, C.M., H.J. Carroll, and D.C. Whiteman, *Estimating the attributable fraction for cancer: A meta-analysis of nevi and melanoma.* Cancer Prev Res (Phila), 2010. **3**(2): p. 233-45.

13. Zhang, T., J. Choi, M.A. Kovacs, J. Shi, M. Xu, N.C.S. Program, C. Melanoma Meta-Analysis, A.M. Goldstein, A.J. Trower, D.T. Bishop, M.M. Iles, D.L. Duffy, S. MacGregor, L.T. Amundadottir, M.H. Law, S.K. Loftus, W.J. Pavan, and K.M. Brown, *Cell-type-specific eQTL of primary melanocytes facilitates identification of melanoma susceptibility genes.* Genome Res, 2018. **28**(11): p. 1621-1635.

14. Cancer Genome Atlas, N., *Genomic Classification of Cutaneous Melanoma.* Cell, 2015. **161**(7): p. 1681-96.

15. Gong, J., S. Mei, C. Liu, Y. Xiang, Y. Ye, Z. Zhang, J. Feng, R. Liu, L. Diao, A.Y. Guo, X. Miao, and L. Han, *PancanQTL: systematic identification of cis-eQTLs and trans-eQTLs in 33 cancer types.* Nucleic Acids Res, 2018. **46**(D1): p. D971-D976.

16. Zhang, T., J. Choi, R. Dilshat, B.O. Einarsdottir, M.A. Kovacs, M. Xu, M. Malasky, S. Chowdhury, K. Jones, D.T. Bishop, A.M. Goldstein, M.M. Iles, M.T. Landi, M.H. Law, J. Shi, E. Steingrimsson, and K.M. Brown, *Cell-type-specific meQTLs extend melanoma GWAS annotation beyond eQTLs and inform melanocyte gene-regulatory mechanisms.* Am J Hum Genet, 2021. **108**(9): p. 1631-1646.

17. Roadmap Epigenomics, C., A. Kundaje, W. Meuleman, J. Ernst, M. Bilenky, A. Yen, A. Heravi-Moussavi, P. Kheradpour, Z. Zhang, J. Wang, M.J. Ziller, V. Amin, J.W. Whitaker, M.D. Schultz, L.D. Ward, A. Sarkar, G. Quon, R.S. Sandstrom, M.L. Eaton, Y.C. Wu, A.R. Pfenning, X. Wang, M. Claussnitzer, Y. Liu, C. Coarfa, R.A. Harris, N. Shoresh, C.B. Epstein, E. Gjoneska, D. Leung, W. Xie, R.D. Hawkins, R. Lister, C. Hong, P. Gascard, A.J. Mungall, R. Moore, E. Chuah, A. Tam, T.K. Canfield, R.S. Hansen, R. Kaul, P.J. Sabo, M.S. Bansal, A. Carles, J.R. Dixon, K.H. Farh, S. Feizi,

R. Karlic, A.R. Kim, A. Kulkarni, D. Li, R. Lowdon, G. Elliott, T.R. Mercer, S.J. Neph, V. Onuchic, P. Polak, N. Rajagopal, P. Ray, R.C. Sallari, K.T. Siebenthall, N.A. Sinnott-Armstrong, M. Stevens, R.E. Thurman, J. Wu, B. Zhang, X. Zhou, A.E. Beaudet, L.A. Boyer, P.L. De Jager, P.J. Farnham, S.J. Fisher, D. Haussler, S.J. Jones, W. Li, M.A. Marra, M.T. McManus, S. Sunyaev, J.A. Thomson, T.D. Tlsty, L.H. Tsai, W. Wang, R.A. Waterland, M.Q. Zhang, L.H. Chadwick, B.E. Bernstein, J.F. Costello, J.R. Ecker, M. Hirst, A. Meissner, A. Milosavljevic, B. Ren, J.A. Stamatoyannopoulos, T. Wang, and M. Kellis, *Integrative analysis of 111 reference human epigenomes.* Nature, 2015. **518**(7539): p. 317-30.

18. Xu, M., L. Mehl, T. Zhang, R. Thakur, H. Sowards, T. Myers, L. Jessop, A. Chesi, M.E. Johnson, A.D. Wells, H.T. Michael, P. Bunda, K. Jones, H. Higson, R.C. Hennessey, A. Jermusyk, M.A. Kovacs, M.T. Landi, M.M. Iles, A.M. Goldstein, C. Melanoma Meta-Analysis, J. Choi, S.J. Chanock, S.F.A. Grant, R. Chari, G. Merlino, M.H. Law, and K.M. Brown, *A UVB-responsive common variant at chromosome band 7p21.1 confers tanning response and melanoma risk via regulation of the aryl hydrocarbon receptor, AHR.* Am J Hum Genet, 2021. **108**(9): p. 1611-1630.

19. Wouters, J., Z. Kalender-Atak, L. Minnoye, K.I. Spanier, M. De Waegeneer, C. Bravo Gonzalez-Blas, D. Mauduit, K. Davie, G. Hulselmans, A. Najem, M. Dewaele, D. Pedri, F. Rambow, S. Makhzami, V. Christiaens, F. Ceyssens, G. Ghanem, J.C. Marine, S. Poovathingal, and S. Aerts, *Robust gene expression programs underlie recurrent cell states and phenotype switching in melanoma.* Nat Cell Biol, 2020. **22**(8): p. 986-998.

20. Ernst, J. and M. Kellis, *Chromatin-state discovery and genome annotation with ChromHMM.* Nat Protoc, 2017. **12**(12): p. 2478-2492.

21. Fiziev, P., K.C. Akdemir, J.P. Miller, E.Z. Keung, N.S. Samant, S. Sharma, C.A. Natale, C.J. Terranova, M. Maitituoheti, S.B. Amin, E. Martinez-Ledesma, M. Dhamdhere, J.B. Axelrad, A. Shah, C.S. Cheng, H. Mahadeshwar, S. Seth, M.C. Barton, A. Protopopov, K.Y. Tsai, M.A. Davies, B.A. Garcia, I. Amit, L. Chin, J. Ernst, and K. Rai, *Systematic Epigenomic Analysis Reveals Chromatin States Associated with Melanoma Progression.* Cell Rep, 2017. **19**(4): p. 875-889.

22. Thakur, R., M. Xu, H. Sowards, J. Yon, L. Jessop, T. Myers, T. Zhang, R. Chari, E. Long, T. Rehling, R. Hennessey, K. Funderburk, J. Yin, M.J. Machiela, M.E. Johnson, A.D. Wells, A. Chesi, S.F.A. Grant, M.M. Iles, M.T. Landi, M.H. Law, C. Melanoma Meta-Analysis, J. Choi, and K.M. Brown, *Mapping chromatin interactions at melanoma susceptibility loci uncovers distant cis-regulatory gene targets.* Am J Hum Genet, 2025. **112**(7): p. 1625-1648.

23. Long, E., J. Yin, K.M. Funderburk, M. Xu, J. Feng, A. Kane, T. Zhang, T. Myers, A. Golden, R. Thakur, H. Kong, L. Jessop, E.Y. Kim, K. Jones, R. Chari, M.J. Machiela, K. Yu, C. Melanoma Meta-Analysis, M.M. Iles, M.T. Landi, M.H. Law, S.J. Chanock, K.M. Brown, and J. Choi, *Massively parallel reporter assays and variant scoring identified functional variants and target genes for melanoma loci and highlighted cell-type specificity.* Am J Hum Genet, 2022. **109**(12): p. 2210-2229.

24. Choi, J., T. Zhang, A. Vu, J. Ablain, M.M. Makowski, L.M. Colli, M. Xu, R.C. Hennessey, J. Yin, H. Rothschild, C. Grawe, M.A. Kovacs, K.M. Funderburk, M. Brossard, J. Taylor, B. Pasaniuc, R. Chari, S.J. Chanock, C.J. Hoggart, F. Demenais, J.H. Barrett, M.H. Law, M.M. Iles, K. Yu, M. Vermeulen, L.I. Zon, and K.M. Brown, *Massively parallel reporter assays of melanoma risk variants identify MX2 as a gene promoting melanoma.* Nat Commun, 2020. **11**(1): p. 2718.

25. Wang, G., A. Sarkar, P. Carbonetto, and M. Stephens, *A simple new approach to variable selection in regression, with application to genetic fine mapping.* J R Stat Soc Series B Stat Methodol, 2020. **82**(5): p. 1273-1300.

26. Zou, Y., P. Carbonetto, G. Wang, and M. Stephens, *Fine-mapping from summary data with the "Sum of Single Effects" model.* PLoS Genet, 2022. **18**(7): p. e1010299.

27. Lee, Y., F. Luca, R. Pique-Regi, and X. Wen, *Bayesian Multi-SNP Genetic Association Analysis: Control of FDR and Use of Summary Statistics.* bioRxiv, 2018: p. 316471.
28. Wen, X., Y. Lee, F. Luca, and R. Pique-Regi, *Efficient Integrative Multi-SNP Association Analysis via Deterministic Approximation of Posteriors.* Am J Hum Genet, 2016. **98**(6): p. 1114-1129.
29. Zhang, W., T. Lu, R. Sladek, J. Dupuis, and G. Lettre, *Robust fine-mapping in the presence of linkage disequilibrium mismatch.* bioRxiv, 2024: p. 2024.10.29.620968.
30. Genomes Project, C., A. Auton, L.D. Brooks, R.M. Durbin, E.P. Garrison, H.M. Kang, J.O. Korbel, J.L. Marchini, S. McCarthy, G.A. McVean, and G.R. Abecasis, *A global reference for human genetic variation.* Nature, 2015. **526**(7571): p. 68-74.
31. Machiela, M.J. and S.J. Chanock, *LDlink: a web-based application for exploring population-specific haplotype structure and linking correlated alleles of possible functional variants.* Bioinformatics, 2015. **31**(21): p. 3555-7.
32. Machiela, M.J. and S.J. Chanock, *LDassoc: an online tool for interactively exploring genome-wide association study results and prioritizing variants for functional investigation.* Bioinformatics, 2018. **34**(5): p. 887-889.
33. Myers, T.A., S.J. Chanock, and M.J. Machiela, *LDlinkR: An R Package for Rapidly Calculating Linkage Disequilibrium Statistics in Diverse Populations.* Front Genet, 2020. **11**: p. 157.
34. Yang, J., S.H. Lee, M.E. Goddard, and P.M. Visscher, *GCTA: a tool for genome-wide complex trait analysis.* Am J Hum Genet, 2011. **88**(1): p. 76-82.
35. Yang, J., T. Ferreira, A.P. Morris, S.E. Medland, A.T.C. Genetic Investigation of, D.I.G. Replication, C. Meta-analysis, P.A. Madden, A.C. Heath, N.G. Martin, G.W. Montgomery, M.N. Weedon, R.J. Loos, T.M. Frayling, M.I. McCarthy, J.N. Hirschhorn, M.E. Goddard, and P.M. Visscher, *Conditional and joint multiple-SNP analysis of GWAS summary statistics identifies additional variants influencing complex traits.* Nat Genet, 2012. **44**(4): p. 369-75, S1-3.
36. Quinlan, A.R. and I.M. Hall, *BEDTools: a flexible suite of utilities for comparing genomic features.* Bioinformatics, 2010. **26**(6): p. 841-2.
37. Patwardhan, M.N., C.D. Wenger, E.S. Davis, and D.H. Phanstiel, *Bedtoolsr: An R package for genomic data analysis and manipulation.* J Open Source Softw, 2019. **4**(44).
38. McLaren, W., L. Gil, S.E. Hunt, H.S. Riat, G.R. Ritchie, A. Thormann, P. Flicek, and F. Cunningham, *The Ensembl Variant Effect Predictor.* Genome Biol, 2016. **17**(1): p. 122.
39. Halaban, R., E. Cheng, Y. Smicun, and J. Germino, *Deregulated E2F transcriptional activity in autonomously growing melanoma cells.* J Exp Med, 2000. **191**(6): p. 1005-16.
40. Agarwal, V., G.W. Bell, J.W. Nam, and D.P. Bartel, *Predicting effective microRNA target sites in mammalian mRNAs.* Elife, 2015. **4**.
41. Huang, H.Y., Y.C. Lin, S. Cui, Y. Huang, Y. Tang, J. Xu, J. Bao, Y. Li, J. Wen, H. Zuo, W. Wang, J. Li, J. Ni, Y. Ruan, L. Li, Y. Chen, Y. Xie, Z. Zhu, X. Cai, X. Chen, L. Yao, Y. Chen, Y. Luo, S. LuXu, M. Luo, C.M. Chiu, K. Ma, L. Zhu, G.J. Cheng, C. Bai, Y.C. Chiang, L. Wang, F. Wei, T.Y. Lee, and H.D. Huang, *miRTarBase update 2022: an informative resource for experimentally validated miRNA-target interactions.* Nucleic Acids Res, 2022. **50**(D1): p. D222-D230.
42. Chen, Y. and X. Wang, *miRDB: an online database for prediction of functional microRNA targets.* Nucleic Acids Res, 2020. **48**(D1): p. D127-D131.
43. Liu, W. and X. Wang, *Prediction of functional microRNA targets by integrative modeling of microRNA binding and target expression data.* Genome Biol, 2019. **20**(1): p. 18.
44. Jeggari, A., D.S. Marks, and E. Larsson, *miRcode: a map of putative microRNA target sites in the long non-coding transcriptome.* Bioinformatics, 2012. **28**(15): p. 2062-3.

45. Fallmann, J., V. Sedlyarov, A. Tanzer, P. Kovarik, and I.L. Hofacker, *ARExite2: an enhanced database for the comprehensive investigation of AU/GU/U-rich elements.* Nucleic Acids Res, 2016. **44**(D1): p. D90-5.
46. Fehlmann, T., F. Kern, O. Laham, C. Backes, J. Solomon, P. Hirsch, C. Volz, R. Muller, and A. Keller, *miRMaster 2.0: multi-species non-coding RNA sequencing analyses at scale.* Nucleic Acids Res, 2021. **49**(W1): p. W397-W408.
47. Langmead, B., C. Trapnell, M. Pop, and S.L. Salzberg, *Ultrafast and memory-efficient alignment of short DNA sequences to the human genome.* Genome Biol, 2009. **10**(3): p. R25.
48. Kozomara, A. and S. Griffiths-Jones, *miRBase: integrating microRNA annotation and deep-sequencing data.* Nucleic Acids Res, 2011. **39**(Database issue): p. D152-7.
49. Kozomara, A. and S. Griffiths-Jones, *miRBase: annotating high confidence microRNAs using deep sequencing data.* Nucleic Acids Res, 2014. **42**(Database issue): p. D68-73.
50. Kozomara, A., M. Birgaoanu, and S. Griffiths-Jones, *miRBase: from microRNA sequences to function.* Nucleic Acids Res, 2019. **47**(D1): p. D155-D162.
51. Griffiths-Jones, S., R.J. Grocock, S. van Dongen, A. Bateman, and A.J. Enright, *miRBase: microRNA sequences, targets and gene nomenclature.* Nucleic Acids Res, 2006. **34**(Database issue): p. D140-4.
52. Ambros, V., B. Bartel, D.P. Bartel, C.B. Burge, J.C. Carrington, X. Chen, G. Dreyfuss, S.R. Eddy, S. Griffiths-Jones, M. Marshall, M. Matzke, G. Ruvkun, and T. Tuschl, *A uniform system for microRNA annotation.* RNA, 2003. **9**(3): p. 277-9.
53. Griffiths-Jones, S., H.K. Saini, S. van Dongen, and A.J. Enright, *miRBase: tools for microRNA genomics.* Nucleic Acids Res, 2008. **36**(Database issue): p. D154-8.
54. Wallace, C., *A more accurate method for colocalisation analysis allowing for multiple causal variants.* PLoS Genet, 2021. **17**(9): p. e1009440.
55. Zhang, W., T. Lu, R. Sladek, Y. Li, H. Najafabadi, and J. Dupuis, *SharePro: an accurate and efficient genetic colocalization method accounting for multiple causal signals.* Bioinformatics, 2024. **40**(5).
56. Gusev, A., A. Ko, H. Shi, G. Bhatia, W. Chung, B.W. Penninx, R. Jansen, E.J. de Geus, D.I. Boomsma, F.A. Wright, P.F. Sullivan, E. Nikkola, M. Alvarez, M. Civelek, A.J. Lusis, T. Lehtimaki, E. Raitoharju, M. Kahonen, I. Seppala, O.T. Raitakari, J. Kuusisto, M. Laakso, A.L. Price, P. Pajukanta, and B. Pasaniuc, *Integrative approaches for large-scale transcriptome-wide association studies.* Nat Genet, 2016. **48**(3): p. 245-52.
57. Wingett, S., P. Ewels, M. Furlan-Magaril, T. Nagano, S. Schoenfelder, P. Fraser, and S. Andrews, *HiCUP: pipeline for mapping and processing Hi-C data.* F1000Res, 2015. **4**: p. 1310.
58. Langmead, B. and S.L. Salzberg, *Fast gapped-read alignment with Bowtie 2.* Nat Methods, 2012. **9**(4): p. 357-9.
59. Cairns, J., P. Freire-Pritchett, S.W. Wingett, C. Varnai, A. Dimond, V. Plagnol, D. Zerbino, S. Schoenfelder, B.M. Javierre, C. Osborne, P. Fraser, and M. Spivakov, *CHiCAGO: robust detection of DNA looping interactions in Capture Hi-C data.* Genome Biol, 2016. **17**(1): p. 127.
60. Li, D., S. Hsu, D. Purushotham, R.L. Sears, and T. Wang, *WashU Epigenome Browser update 2019.* Nucleic Acids Res, 2019. **47**(W1): p. W158-W165.
61. Li, D., D. Purushotham, J.K. Harrison, S. Hsu, X. Zhuo, C. Fan, S. Liu, V. Xu, S. Chen, J. Xu, S. Ouyang, A.S. Wu, and T. Wang, *WashU Epigenome Browser update 2022.* Nucleic Acids Res, 2022. **50**(W1): p. W774-W781.
62. Kent, W.J., C.W. Sugnet, T.S. Furey, K.M. Roskin, T.H. Pringle, A.M. Zahler, and D. Haussler, *The human genome browser at UCSC.* Genome Res, 2002. **12**(6): p. 996-1006.
63. Lee, B.T., G.P. Barber, A. Benet-Pages, J. Casper, H. Clawson, M. Diekhans, C. Fischer, J.N. Gonzalez, A.S. Hinrichs, C.M. Lee, P. Muthuraman, L.R. Nassar, B. Nguy, T. Pereira, G. Perez, B.J. Raney, K.R. Rosenbloom, D. Schmelter, M.L. Speir,

B.D. Wick, A.S. Zweig, D. Haussler, R.M. Kuhn, M. Haeussler, and W.J. Kent, *The UCSC Genome Browser database: 2022 update.* Nucleic Acids Res, 2022. **50**(D1): p. D1115-D1122.

64. Navarro Gonzalez, J., A.S. Zweig, M.L. Speir, D. Schmelter, K.R. Rosenbloom, B.J. Raney, C.C. Powell, L.R. Nassar, N.D. Maulding, C.M. Lee, B.T. Lee, A.S. Hinrichs, A.C. Fyfe, J.D. Fernandes, M. Diekhans, H. Clawson, J. Casper, A. Benet-Pages, G.P. Barber, D. Haussler, R.M. Kuhn, M. Haeussler, and W.J. Kent, *The UCSC Genome Browser database: 2021 update.* Nucleic Acids Res, 2021. **49**(D1): p. D1046-D1057.

65. Raney, B.J., T.R. Dreszer, G.P. Barber, H. Clawson, P.A. Fujita, T. Wang, N. Nguyen, B. Paten, A.S. Zweig, D. Karolchik, and W.J. Kent, *Track data hubs enable visualization of user-defined genome-wide annotations on the UCSC Genome Browser.* Bioinformatics, 2014. **30**(7): p. 1003-5.

66. Rosenbloom, K.R., C.A. Sloan, V.S. Malladi, T.R. Dreszer, K. Learned, V.M. Kirkup, M.C. Wong, M. Maddren, R. Fang, S.G. Heitner, B.T. Lee, G.P. Barber, R.A. Harte, M. Diekhans, J.C. Long, S.P. Wilder, A.S. Zweig, D. Karolchik, R.M. Kuhn, D. Haussler, and W.J. Kent, *ENCODE data in the UCSC Genome Browser: year 5 update.* Nucleic Acids Res, 2013. **41**(Database issue): p. D56-63.

67. Ceol, C.J., Y. Houvras, J. Jane-Valbuena, S. Bilodeau, D.A. Orlando, V. Battisti, L. Fritsch, W.M. Lin, T.J. Hollmann, F. Ferre, C. Bourque, C.J. Burke, L. Turner, A. Uong, L.A. Johnson, R. Beroukhim, C.H. Mermel, M. Loda, S. Ait-Si-Ali, L.A. Garraway, R.A. Young, and L.I. Zon, *The histone methyltransferase SETDB1 is recurrently amplified in melanoma and accelerates its onset.* Nature, 2011. **471**(7339): p. 513-7.

68. Ablain, J., M. Xu, H. Rothschild, R.C. Jordan, J.K. Mito, B.H. Daniels, C.F. Bell, N.M. Joseph, H. Wu, B.C. Bastian, L.I. Zon, and I. Yeh, *Human tumor genomics and zebrafish modeling identify SPRED1 loss as a driver of mucosal melanoma.* Science, 2018. **362**(6418): p. 1055-1060.

69. Birkealv, S., M. Harland, L. Matsuyama, M. Rashid, I. Mehta, J.P. Laye, K. Haase, T. Mell, V. Iyer, C.D. Robles-Espinoza, U. McDermott, P. van Loo, M.L. Kuijjer, P.A. Possik, S.S. Maria Engler, D.T. Bishop, J. Newton-Bishop, and D.J. Adams, *Mutually exclusive genetic interactions and gene essentiality shape the genomic landscape of primary melanoma.* J Pathol, 2023. **259**(1): p. 56-68.

70. Nsengimana, J., J. Laye, A. Filia, S. O'Shea, S. Muralidhar, J. Pozniak, A. Droop, M. Chan, C. Walker, L. Parkinson, J. Gascoyne, T. Mell, M. Polso, R. Jewell, J. Randerson-Moor, G.P. Cook, D.T. Bishop, and J. Newton-Bishop, *beta-Catenin-mediated immune evasion pathway frequently operates in primary cutaneous melanomas.* J Clin Invest, 2018. **128**(5): p. 2048-2063.

71. Thakur, R., J.P. Laye, M. Lauss, J.M.S. Diaz, S.J. O'Shea, J. Pozniak, A. Filia, M. Harland, J. Gascoyne, J.A. Randerson-Moor, M. Chan, T. Mell, G. Jonsson, D.T. Bishop, J. Newton-Bishop, J.H. Barrett, and J. Nsengimana, *Transcriptomic Analysis Reveals Prognostic Molecular Signatures of Stage I Melanoma.* Clin Cancer Res, 2019. **25**(24): p. 7424-7435.

72. Cirenajwis, H., M. Lauss, H. Ekedahl, T. Torngren, A. Kvist, L.H. Saal, H. Olsson, J. Staaf, A. Carneiro, C. Ingvar, K. Harbst, N.K. Hayward, and G. Jonsson, *NF1-mutated melanoma tumors harbor distinct clinical and biological characteristics.* Mol Oncol, 2017. **11**(4): p. 438-451.

73. Liu, D., B. Schilling, D. Liu, A. Sucker, E. Livingstone, L. Jerby-Arnon, L. Zimmer, R. Gutzmer, I. Satzger, C. Loquai, S. Grabbe, N. Vokes, C.A. Margolis, J. Conway, M.X. He, H. Elmarakeby, F. Dietlein, D. Miao, A. Tracy, H. Gogas, S.M. Goldinger, J. Utikal, C.U. Blank, R. Rauschenberg, D. von Bubnoff, A. Krackhardt, B. Weide, S. Haferkamp, F. Kiecker, B. Izar, L. Garraway, A. Regev, K. Flaherty, A. Paschen, E.M. Van Allen, and D. Schadendorf, *Integrative molecular and clinical modeling of clinical outcomes to PD1 blockade in patients with metastatic melanoma.* Nat Med, 2019. **25**(12): p. 1916-1927.

74. Van Allen, E.M., D. Miao, B. Schilling, S.A. Shukla, C. Blank, L. Zimmer, A. Sucker, U. Hillen, M.H.G. Foppen, S.M. Goldinger, J. Utikal, J.C. Hassel, B. Weide, K.C. Kaehler, C. Loquai, P. Mohr, R. Gutzmer, R. Dummer, S. Gabriel, C.J. Wu, D. Schadendorf, and L.A. Garraway, *Genomic correlates of response to CTLA-4 blockade in metastatic melanoma.* Science, 2015. **350**(6257): p. 207-211.
75. Riaz, N., J.J. Havel, V. Makarov, A. Desrichard, W.J. Urba, J.S. Sims, F.S. Hodi, S. Martin-Algarra, R. Mandal, W.H. Sharfman, S. Bhatia, W.J. Hwu, T.F. Gajewski, C.L. Slingluff, Jr., D. Chowell, S.M. Kendall, H. Chang, R. Shah, F. Kuo, L.G.T. Morris, J.W. Sidhom, J.P. Schneck, C.E. Horak, N. Weinhold, and T.A. Chan, *Tumor and Microenvironment Evolution during Immunotherapy with Nivolumab.* Cell, 2017. **171**(4): p. 934-949 e16.
76. Hu, J., B. Liu, W. Hu, and Y. Yang, *A pretreatment transcriptomic signature that predicts outcomes of immunotherapy in melanoma.* Heliyon, 2022. **8**(12): p. e12648.
77. Sanchez-Vega, F., M. Mina, J. Armenia, W.K. Chatila, A. Luna, K.C. La, S. Dimitriadoy, D.L. Liu, H.S. Kantheti, S. Saghafinia, D. Chakravarty, F. Daian, Q. Gao, M.H. Bailey, W.W. Liang, S.M. Foltz, I. Shmulevich, L. Ding, Z. Heins, A. Ochoa, B. Gross, J. Gao, H. Zhang, R. Kundra, C. Kandoth, I. Bahceci, L. Dervishi, U. Dogrusoz, W. Zhou, H. Shen, P.W. Laird, G.P. Way, C.S. Greene, H. Liang, Y. Xiao, C. Wang, A. Iavarone, A.H. Berger, T.G. Bivona, A.J. Lazar, G.D. Hammer, T. Giordano, L.N. Kwong, G. McArthur, C. Huang, A.D. Tward, M.J. Frederick, F. McCormick, M. Meyerson, N. Cancer Genome Atlas Research, E.M. Van Allen, A.D. Cherniack, G. Ciriello, C. Sander, and N. Schultz, *Oncogenic Signaling Pathways in The Cancer Genome Atlas.* Cell, 2018. **173**(2): p. 321-337 e10.
78. Balch, C.M., J.E. Gershenwald, S.J. Soong, J.F. Thompson, M.B. Atkins, D.R. Byrd, A.C. Buzaid, A.J. Cochran, D.G. Coit, S. Ding, A.M. Eggermont, K.T. Flaherty, P.A. Gimotty, J.M. Kirkwood, K.M. McMasters, M.C. Mihm, Jr., D.L. Morton, M.I. Ross, A.J. Sober, and V.K. Sondak, *Final version of 2009 AJCC melanoma staging and classification.* J Clin Oncol, 2009. **27**(36): p. 6199-206.
79. Consortium, E.P., J.E. Moore, M.J. Purcaro, H.E. Pratt, C.B. Epstein, N. Shoresh, J. Adrian, T. Kawli, C.A. Davis, A. Dobin, R. Kaul, J. Halow, E.L. Van Nostrand, P. Freese, D.U. Gorkin, Y. Shen, Y. He, M. Mackiewicz, F. Pauli-Behn, B.A. Williams, A. Mortazavi, C.A. Keller, X.O. Zhang, S.I. Elhajjajy, J. Huey, D.E. Dickel, V. Snetkova, X. Wei, X. Wang, J.C. Rivera-Mulia, J. Rozowsky, J. Zhang, S.B. Chhetri, J. Zhang, A. Victorsen, K.P. White, A. Visel, G.W. Yeo, C.B. Burge, E. Lecuyer, D.M. Gilbert, J. Dekker, J. Rinn, E.M. Mendenhall, J.R. Ecker, M. Kellis, R.J. Klein, W.S. Noble, A. Kundaje, R. Guigo, P.J. Farnham, J.M. Cherry, R.M. Myers, B. Ren, B.R. Graveley, M.B. Gerstein, L.A. Pennacchio, M.P. Snyder, B.E. Bernstein, B. Wold, R.C. Hardison, T.R. Gingeras, J.A. Stamatoyannopoulos, and Z. Weng, *Expanded encyclopaedias of DNA elements in the human and mouse genomes.* Nature, 2020. **583**(7818): p. 699-710.
80. Chen, C., Y. Liu, M. Luo, J. Yang, Y. Chen, R. Wang, J. Zhou, Y. Zang, L. Diao, and L. Han, *PancanQTLv2.0: a comprehensive resource for expression quantitative trait loci across human cancers.* Nucleic Acids Res, 2024. **52**(D1): p. D1400-D1406.
81. Garraway, L.A., H.R. Widlund, M.A. Rubin, G. Getz, A.J. Berger, S. Ramaswamy, R. Beroukhim, D.A. Milner, S.R. Granter, J. Du, C. Lee, S.N. Wagner, C. Li, T.R. Golub, D.L. Rimm, M.L. Meyerson, D.E. Fisher, and W.R. Sellers, *Integrative genomic analyses identify MITF as a lineage survival oncogene amplified in malignant melanoma.* Nature, 2005. **436**(7047): p. 117-22.
82. Choi, J., M. Xu, M.M. Makowski, T. Zhang, M.H. Law, M.A. Kovacs, A. Granzhan, W.J. Kim, H. Parikh, M. Gartside, J.M. Trent, M.P. Teulade-Fichou, M.M. Iles, J.A. Newton-Bishop, D.T. Bishop, S. MacGregor, N.K. Hayward, M. Vermeulen, and K.M. Brown, *A common intronic variant of PARP1 confers melanoma risk and mediates melanocyte growth via regulation of MITF.* Nat Genet, 2017. **49**(9): p. 1326-1335.
83. Carr, R.M., D. Vorobyev, T. Lasho, D.L. Marks, E.J. Tolosa, A. Vedder, L.L. Almada, A. Yurcheko, I. Padioleau, B. Alver, G. Coltro, M. Binder, S.L. Safgren, I. Horn, X.

You, E. Solary, M.E. Balasis, K. Berger, J. Hiebert, T. Witzig, A. Buradkar, T. Graf, P. Valent, A.A. Mangaonkar, K.D. Robertson, M.T. Howard, S.H. Kaufmann, C. Pin, M.E. Fernandez-Zapico, K. Geissler, N. Droin, E. Padron, J. Zhang, S. Nikolaev, and M.M. Patnaik, *RAS mutations drive proliferative chronic myelomonocytic leukemia via a KMT2A-PLK1 axis.* Nat Commun, 2021. **12**(1): p. 2901.

84. Eisfeld, A.K., S. Schwind, K.W. Hoag, C.J. Walker, S. Liyanarachchi, R. Patel, X. Huang, J. Markowitz, W. Duan, G.A. Otterson, W.E. Carson, 3rd, G. Marcucci, C.D. Bloomfield, and A. de la Chapelle, *NRAS isoforms differentially affect downstream pathways, cell growth, and cell transformation.* Proc Natl Acad Sci U S A, 2014. **111**(11): p. 4179-84.

85. Burd, C.E., W. Liu, M.V. Huynh, M.A. Waqas, J.E. Gillahan, K.S. Clark, K. Fu, B.L. Martin, W.R. Jeck, G.P. Souroullas, D.B. Darr, D.C. Zedek, M.J. Miley, B.C. Baguley, S.L. Campbell, and N.E. Sharpless, *Mutation-specific RAS oncogenicity explains NRAS codon 61 selection in melanoma.* Cancer Discov, 2014. **4**(12): p. 1418-29.

86. Popovic, M., M. Rensen-de Leeuw, and H. Rehmann, *Selectivity of CDC25 homology domain-containing guanine nucleotide exchange factors.* J Mol Biol, 2013. **425**(15): p. 2782-94.

87. Gotoh, T., Y. Niino, M. Tokuda, O. Hatase, S. Nakamura, M. Matsuda, and S. Hattori, *Activation of R-Ras by Ras-guanine nucleotide-releasing factor.* J Biol Chem, 1997. **272**(30): p. 18602-7.

88. Frech, M., J. John, V. Pizon, P. Chardin, A. Tavitian, R. Clark, F. McCormick, and A. Wittinghofer, *Inhibition of GTPase activating protein stimulation of Ras-p21 GTPase by the Krev-1 gene product.* Science, 1990. **249**(4965): p. 169-71.

89. Ohba, Y., K. Kurokawa, and M. Matsuda, *Mechanism of the spatio-temporal regulation of Ras and Rap1.* EMBO J, 2003. **22**(4): p. 859-69.

90. Lopez-Bergami, P., B. Fitchman, and Z. Ronai, *Understanding signaling cascades in melanoma.* Photochem Photobiol, 2008. **84**(2): p. 289-306.

91. Savoia, P., P. Fava, F. Casoni, and O. Cremona, *Targeting the ERK Signaling Pathway in Melanoma.* Int J Mol Sci, 2019. **20**(6).

92. Al Mahi, A. and J. Ablain, *RAS pathway regulation in melanoma.* Dis Model Mech, 2022. **15**(2).

93. Prior, I.A., F.E. Hood, and J.L. Hartley, *The Frequency of Ras Mutations in Cancer.* Cancer Res, 2020. **80**(14): p. 2969-2974.

94. Pipek, O., L. Vizkeleti, V. Doma, D. Alpar, C. Bodor, S. Karpati, and J. Timar, *The Driverless Triple-Wild-Type (BRAF, RAS, KIT) Cutaneous Melanoma: Whole Genome Sequencing Discoveries.* Cancers (Basel), 2023. **15**(6).

95. Luo, L., R. Shen, A. Arora, I. Orlow, K.J. Busam, C. Lezcano, T.K. Lee, E. Hernando, I. Gorlov, C. Amos, M.S. Ernstoff, V.E. Seshan, A.E. Cust, J. Wilmott, R.A. Scolyer, G. Mann, E. Nagore, P. Funchain, J. Ko, P. Ngo, S.N. Edmiston, K. Conway, P.B. Googe, D. Ollila, J.E. Lee, S. Fang, J.R. Rees, C.L. Thompson, M. Gerstenblith, M. Bosenberg, B. Gould Rothberg, I. Osman, Y. Saenger, A.Z. Reynolds, M. Schwartz, T. Boyce, S. Holmen, E. Brunsgaard, P. Bogner, P.F. Kuan, C. Wiggins, N.E. Thomas, C.B. Begg, M. Berwick, and InterMel, *Landscape of mutations in early stage primary cutaneous melanoma: An InterMEL study.* Pigment Cell Melanoma Res, 2022. **35**(6): p. 605-612.

96. Conway, J.R., F. Dietlein, A. Taylor-Weiner, S. AlDubayan, N. Vokes, T. Keenan, B. Reardon, M.X. He, C.A. Margolis, J.L. Weirather, R. Haq, B. Schilling, F. Stephen Hodi, D. Schadendorf, D. Liu, and E.M. Van Allen, *Integrated molecular drivers coordinate biological and clinical states in melanoma.* Nat Genet, 2020. **52**(12): p. 1373-1383.

97. Ehrhardt, A., G.R. Ehrhardt, X. Guo, and J.W. Schrader, *Ras and relatives--job sharing and networking keep an old family together.* Exp Hematol, 2002. **30**(10): p. 1089-106.

98. Vigil, D., J. Cherfils, K.L. Rossman, and C.J. Der, *Ras superfamily GEFs and GAPs: validated and tractable targets for cancer therapy?* Nat Rev Cancer, 2010. **10**(12): p. 842-57.
99. Rebhun, J.F., A.F. Castro, and L.A. Quilliam, *Identification of guanine nucleotide exchange factors (GEFs) for the Rap1 GTPase. Regulation of MR-GEF by M-Ras-GTP interaction.* J Biol Chem, 2000. **275**(45): p. 34901-8.
100. Yamashita, S., N. Mochizuki, Y. Ohba, M. Tobiume, Y. Okada, H. Sawa, K. Nagashima, and M. Matsuda, *CalDAG-GEFIII activation of Ras, R-ras, and Rap1.* J Biol Chem, 2000. **275**(33): p. 25488-93.
101. Clyde-Smith, J., G. Silins, M. Gartside, S. Grimmond, M. Etheridge, A. Apolloni, N. Hayward, and J.F. Hancock, *Characterization of RasGRP2, a plasma membrane-targeted, dual specificity Ras/Rap exchange factor.* J Biol Chem, 2000. **275**(41): p. 32260-7.
102. Ishimaru, S., R. Williams, E. Clark, H. Hanafusa, and U. Gaul, *Activation of the Drosophila C3G leads to cell fate changes and overproliferation during development, mediated by the RAS-MAPK pathway and RAP1.* EMBO J, 1999. **18**(1): p. 145-55.
103. Kelly, M.R., K. Kostyrko, K. Han, N.A. Mooney, E.E. Jeng, K. Spees, P.T. Dinh, K.L. Abbott, D.M. Gwinn, E.A. Sweet-Cordero, M.C. Bassik, and P.K. Jackson, *Combined Proteomic and Genetic Interaction Mapping Reveals New RAS Effector Pathways and Susceptibilities.* Cancer Discov, 2020. **10**(12): p. 1950-1967.
104. Kovalski, J.R., A. Bhaduri, A.M. Zehnder, P.H. Neela, Y. Che, G.G. Wozniak, and P.A. Khavari, *The Functional Proximal Proteome of Oncogenic Ras Includes mTORC2.* Mol Cell, 2019. **73**(4): p. 830-844 e12.
105. Carabias, A., M. Gomez-Hernandez, S. de Cima, A. Rodriguez-Blazquez, A. Moran-Vaquero, P. Gonzalez-Saenz, C. Guerrero, and J.M. de Pereda, *Mechanisms of autoregulation of C3G, activator of the GTPase Rap1, and its catalytic deregulation in lymphomas.* Sci Signal, 2020. **13**(647).
106. Rauen, K.A., *The RASopathies.* Annu Rev Genomics Hum Genet, 2013. **14**: p. 355-69.
107. Kiuru, M., J. Urban, G. Zhu, I. Rybak, J.R. Terrell, L. Qi, J.D. McPherson, A.A. Marghoob, and K.A. Rauen, *RAS pathway influences the number of melanocytic nevi in cardiofaciocutaneous and Costello syndromes.* J Am Acad Dermatol, 2020. **82**(5): p. 1091-1093.
108. Siegel, D.H., J. McKenzie, I.J. Frieden, and K.A. Rauen, *Dermatological findings in 61 mutation-positive individuals with cardiofaciocutaneous syndrome.* Br J Dermatol, 2011. **164**(3): p. 521-9.
109. Vaughn, A.R., S.N. Meyer, Z.H. Nazir, J. Tavernetti, E. Simmons, H. Li, I. Rybak, K.A. Rauen, A.A. Marghoob, and M. Kiuru, *Dermoscopic Features of Melanocytic Nevi in Cardiofaciocutaneous and Costello Syndromes.* JAMA Dermatol, 2024. **160**(8): p. 869-873.
110. Ahmed, S.B.M. and S.A. Prigent, *Insights into the Shc Family of Adaptor Proteins.* J Mol Signal, 2017. **12**: p. 2.
111. Gu, H., H. Maeda, J.J. Moon, J.D. Lord, M. Yoakim, B.H. Nelson, and B.G. Neel, *New role for Shc in activation of the phosphatidylinositol 3-kinase/Akt pathway.* Mol Cell Biol, 2000. **20**(19): p. 7109-20.
112. Jayasinghe, G.J.M.S.R., G. Zhu, N. Pandeya, C.M. Olsen, N.G. Martin, P.A. Lind, S.E. Medland, S.D. Gordon, S.D. Torres, G. Lingham, S.S.Y. Lee, T. Nijsten, M. Kayser, L.M. Pardo, G.W. Montgomery, N.K. Hayward, J.M. Palmer, D.J. Hunter, J. Han, A.W. Hewitt, M. Falchi, D.T. Bishop, K.M. Brown, V. Bataille, D.A. Mackey, M.M. Iles, D.C. Whiteman, D.L. Duffy, S. MacGregor, and M.H. Law, *A large-scale genome-wide association meta-analysis for nevus count provides direct insights into the genetics of melanoma.* medRxiv, 2025: p. 2025.02.25.25322831.